

JGR Atmospheres

RESEARCH ARTICLE

10.1029/2021JD034691

Key Points:

- Trends (1998–2019) in free troposphere (FT) O₃ at five SHADOZ sites are ~(-1–4)%/decade, lower than some satellite or aircraft profile estimates
- Corresponding lowermost stratospheric (LMS) O₃ changes are ~(-3)%/decade, coinciding with an increase in tropopause height
- Both FT and LMS O₃ trends vary seasonally and regionally, defining new references for evaluating assessment models and satellite products

Supporting Information:

Supporting Information may be found in the online version of this article.

Correspondence to:

A. M. Thompson,
anne.m.thompson@nasa.gov

Citation:

Thompson, A. M., Stauffer, R. M., Wargan, K., Witte, J. C., Kollonige, D. E., & Ziemke, J. R. (2021). Regional and seasonal trends in tropical ozone from SHADOZ profiles: Reference for models and satellite products. *Journal of Geophysical Research: Atmospheres*, 126, e2021JD034691. <https://doi.org/10.1029/2021JD034691>

Received 30 JAN 2021
Accepted 12 OCT 2021

Author Contributions:

Conceptualization: Anne M. Thompson
Data curation: Anne M. Thompson, Jacquelyn C. Witte, Debra E. Kollonige
Formal analysis: Ryan M. Stauffer, Jacquelyn C. Witte
Funding acquisition: Anne M. Thompson
Investigation: Anne M. Thompson
Methodology: Anne M. Thompson, Krzysztof Wargan, Jerald R. Ziemke
Project Administration: Anne M. Thompson
Resources: Anne M. Thompson
Software: Ryan M. Stauffer, Jacquelyn C. Witte, Jerald R. Ziemke

Regional and Seasonal Trends in Tropical Ozone From SHADOZ Profiles: Reference for Models and Satellite Products

Anne M. Thompson^{1,2} , Ryan M. Stauffer¹ , Krzysztof Wargan^{1,3} , Jacquelyn C. Witte⁴ , Debra E. Kollonige^{1,3} , and Jerald R. Ziemke^{1,5} 

¹NASA/Goddard Space Flight Center (GSFC), Greenbelt, MD, USA, ²Joint Center for Earth Systems Technology (JCET)/University of Maryland-Baltimore County, Baltimore, MD, USA, ³Science Systems and Applications, Inc., Lanham, MD, USA, ⁴National Center for Atmospheric Research Earth Observations Laboratory, Boulder, CO, USA, ⁵Morgan State University, Baltimore, MD, USA

Abstract Understanding lowermost stratosphere (LMS) ozone variability is an important topic in the trends and climate assessment communities because of feedbacks among changing temperature, dynamics, and ozone. LMS evaluations are usually based on satellite observations. Free tropospheric (FT) ozone assessments typically rely on profiles from commercial aircraft. Ozone sonde measurements constitute an independent data set encompassing both LMS and FT. We used Southern Hemisphere Additional Ozone sondes (SHADOZ) data (5.8°N–14°S) from 1998 to 2019 in the Goddard Multiple Linear Regression model to analyze monthly mean FT and LMS ozone changes across five well-distributed tropical sites. Our findings: (a) both FT (5–15 km) and LMS (15–20 km) ozone trends show marked seasonal variability. (b) All stations exhibit FT ozone increases in February–May (up to 15%/decade) when the frequency of convectively driven waves have changed. (c) After May, monthly ozone changes are both positive and negative, leading to mean trends of +(1–4)%/decade, depending on station. (d) LMS ozone losses reach (4–9)%/decade midyear, correlating with an increase in TH as derived from SHADOZ radiosonde data. (e) When the upper FT and LMS are defined by tropopause-relative coordinates, the LMS ozone trends all become insignificant. Thus, the 20-year decline in tropical LMS ozone reported in recent satellite-based studies likely signifies a perturbed tropopause rather than chemical depletion. The SHADOZ-derived ozone changes highlight regional and seasonal variability across the tropics and define a new reference for evaluating changes derived from models and satellite products over the 1998–2019 period.

Plain Language Summary Understanding free troposphere (FT) and lowermost stratosphere (LMS) ozone trends is important. If FT ozone increases, it will augment global warming. If LMS ozone has declined in the past 20 years it could mean that something is amiss in atmospheric conditions despite successes of the Montreal Protocol to eliminate ozone-depleting chemicals from the stratosphere. This study used high-accuracy, high-resolution (~150 m) ozone profiles from balloon-borne sondes to determine changes over the tropics. The data come from five sites in the Southern Hemisphere Additional Ozone sondes (SHADOZ) archive covering 1998–2019. A summary of results: (a) both FT (5–15 km) and LMS (15–20 km) ozone trends show marked seasonal variability. (b) All stations exhibit strong positive FT ozone trends in the February–May period but annual means at several stations comparable to the IAGOS record are ≤2%/decade. (c) LMS ozone losses range from (4–9)%/decade midyear and appear to be an artifact of an increasing tropopause height. Therefore, the 20-year decline in tropical LMS ozone published in satellite-based studies may signify a perturbed tropopause, that is, a climate signal. Our SHADOZ-derived ozone trends are available for models, challenging them to reproduce the regional and seasonal variations we find in recent trends.

1. Introduction

1.1. Trends in Free Tropospheric and Lowermost Stratospheric Ozone

Trends in tropical free tropospheric (FT) ozone have been featured in studies that use model results (Zhang et al., 2016), satellite data (Gaudel et al., 2018; Ziemke et al., 2019), and commercial aircraft profiles (Gaudel

Supervision: Anne M. Thompson

Validation: Krzysztof Wargan

Visualization: Ryan M. Stauffer

Writing – original draft: Anne M. Thompson

Writing – review & editing: Anne M. Thompson, Ryan M. Stauffer, Debra E. Kollonige

et al., 2020). Gaudel et al. (2018) summarize global uncertainties, displaying trends in tropical tropospheric ozone from five satellite-derived maps that disagree in magnitude and even sign. Changes based on various Aura/OMI (2005–2016) products ranged from $\sim(5\text{--}25)\%$ /decade. Using commercial aircraft data (<http://iagos.org>; In-service Aircraft for a Global Observing System) from a small number of urban airports in the northern tropics, Gaudel et al. (2020) report trends in tropical FT ozone equivalent to $+(3\text{--}5)\%$ /decade.

Studies with satellite data, including Aura OMI and MLS, also reflect uncertainty in both FT and LMS ozone trends over the past 15–20 years. Recent work with merged satellite data sets (SWOOSH, GOZCARDS, Merged SBUV; SPARC/IO3C/GAW, 2018) in the mid to lower stratosphere, along with chemistry-transport models (Stauffer et al., 2019) and ozone assimilations, indicate the uncertainty of possible LMS ozone trends (Ball et al., 2018; Chipperfield et al., 2018; Wargan et al., 2018), at least on a zonally averaged basis. For example, the products summarized by Ball et al. (2018), suggest a 20-year (1998–2016) lowermost stratospheric (LMS) ozone loss up to 3% /decade, whereas Wargan et al. (2018; their Figure 3) show a comparable increase in tropical LMS ozone over the same period. A new study (Szelag et al., 2020) with four satellite products reports LMS ozone losses of $(2\text{--}3)\%$ /decade in the tropics, a value that agrees with the most recent analysis of satellite data and with many models (Ball et al., 2020).

Ozonesonde data are widely used by the scientific community for satellite validation and model evaluation, especially in the region from ~ 5 to 20 km, where uncertainties in most satellite measurements are relatively large and feedbacks among temperature, dynamics, ozone, and water vapor are complex and important. SHADOZ (Southern Hemisphere Additional Ozonesondes; Thompson, Witte, McPeters, et al., 2003; Thompson et al., 2012) is a 14-station tropical and subtropical network that has archived $>9,000$ profiles since 1998. In this study, we determine trends in tropical FT and LMS ozone with reprocessed v06 SHADOZ profiles (Thompson et al., 2017; Witte et al., 2017, 2018) that are better resolved (100–150 m in the vertical) than satellite measurements below 20 km. Thus, with a single data set interannual and seasonal variability throughout the FT, LMS, and the critical tropopause transition layer between them are analyzed. There are other advantages of SHADOZ data. The SHADOZ measurements, distributed across eight tropical stations (Thompson, Witte, McPeters, et al., 2003), capture geographical variability, and cover troposphere and stratosphere with $\sim 5\%$ precision. Most SHADOZ locations are relatively free of urban influence so trends in FT ozone represent changes in background ozone over a large segment of the tropics. Another advantage of the SHADOZ data is that potential temperature readings from the radiosondes accompanying the ozonesonde launches provide direct information on dynamical factors that may be related to oscillations and trends.

1.2. Role of Climate Oscillations and Convection in Tropical Ozone Variability

Early studies of FT and LMS ozone variability with SHADOZ profiles focused on convective influences (Folkins et al., 2000, 2002) and biomass burning (Oltmans et al., 2001) over the western Pacific. More generally, Thompson, Witte, Oltmans, et al. (2003) showed that a mixture of dynamical and chemical influences determines FT ozone seasonal patterns at all SHADOZ stations. This view has been confirmed in studies of field campaigns (Swap et al., 2002; Thouret et al., 2009) and satellite observations (Nassar et al., 2009).

ENSO-perturbed patterns of convection, precipitation, and fire lead to variability in FT and LMS ozone profiles that vary station to station. In some cases, the ENSO leads to positive ozone anomalies; at other locations, ozone may decrease (Randel & Thompson, 2011; Thompson & Hudson, 1999). Thompson et al. (2001) used sonde and satellite data to demonstrate that even when fires cause exceptional pollution, as over Indonesia in 1997–1998, dynamical anomalies like the ENSO and Indian Ocean Dipole are major factors in a tropospheric ozone buildup. Other studies linking dynamics and FT and LMS ozone variability have examined the QBO (Witte et al., 2008). Compared to HALOE on UARS (Halogen Occultation Experiment, Upper Atmosphere Research Satellite), SHADOZ sonde profiles show more structure in the LMS. Employing different statistical approaches, Lee et al. (2010) and Randel and Thompson (2011) found that QBO and ENSO impacts on FT and LMS ozone varied among stations within $\pm 12^\circ$ latitude of the equator over the first 12 years of SHADOZ (1998–2009).

Thompson et al. (2011) reported on convectively generated wave activity in the LMS for 10 stations over the first decade (1998–2007) of the SHADOZ record. Laminae in ozone and potential temperature profiles were

used to identify vertical displacements in segments up to 20 km that are attributed to convectively generated waves (Grant et al., 1998). Using a Gravity Wave Index (GWI) based on laminae frequency, ozone variations were linked to the ENSO cycle (Thompson et al., 2011). Strong relationships between gravity waves and ozone vertical structure are also indicated when FT ozone profiles are classified by Self-Organizing Maps (SOM; Jensen et al., 2012; Stauffer et al., 2018). The lowest-ozone mixing ratios from ~5 to 15 km at SHADOZ stations coincide with the most intense convective activity, as indicated by wind velocity potential, geopotential height, cloud cover, etc. Profiles with the highest-ozone mixing ratios occur under stable meteorological conditions along with elevated concentrations of pollutants as seen by satellite. Signatures of the Madden-Julian Oscillation in ozone variations over the western Pacific/eastern Indian Ocean have been reported in SHADOZ profiles (Stauffer et al., 2018) and in satellite estimations of tropospheric ozone (Ziemke & Chandra, 2003).

1.3. This Study

The uncertainty in lower atmospheric ozone changes over the past two decades and the documented impact of seasonal convection and climate oscillations on tropical ozone are motivation for examining ozone variability and trends with the 22-year SHADOZ record. First, we review seasonal and regional variations in FT and LMS ozone SHADOZ observations and convective activity as signified by ozone and radiosonde laminae. Second, trends in ozone profiles from 1998 to 2019 are determined with a standard Multiple Linear Regression (MLR) model. To investigate possible mechanisms for FT and LMS ozone changes, the MLR model is also applied to tropopause height derived from the SHADOZ radiosondes. We address the following questions:

1. What are the trends, if any, in FT and LMS ozone in the tropics?
2. Are there regional and/or seasonal variations in the trends?
3. Do the sonde data provide useful information on dynamical factors connected to trends?

Depending on the station location we find negligible to small trends in ozone with distinct seasonality over the 22-year period, positive in the FT, and negative in the LMS. The FT changes are strongest in February–May, when ozone is a minimum, and become negative about half the time during the remainder of the year. The LMS trend maximizes mid-year when there is an increasing trend in tropopause height (TH). The monthly averaged ozone and TH data along with the corresponding MLR model best-fit output are available to the satellite and modeling communities as an objective reference for their products. Data and analysis methods appear in Section 2 with Results and Discussion in Section 3. Section 4 is a summary.

2. Data and Methods of Analysis

2.1. FT and LMS Definitions

The analyses below span the surface to 20 km with the main results discussed referring to two FT segments: 5–10 km; 10–15 km. Ozone and pressure-temperature-humidity (P-T-U) data below 5 km are not used because sampling times vary among stations. Station launch times are subject to change; at one SHADOZ station, for example, a trend in boundary-layer ozone was reported that was an artifact of a 5-hr launch change (Clain et al., 2009; Thompson et al., 2014). We use 15–20 km for the LMS, because this is where convective impacts on waves maximize (Thompson et al., 2011) and where Randel et al. (2007) identified a distinct ozone annual cycle driven by the Brewer-Dobson circulation. The LMS includes most of the tropical tropopause layer (13.5–18.5 km) and several km above the tropical cold-point and thermal lapse-rate tropopauses over the SHADOZ sites (Selkirk et al., 2010; Thompson et al., 2012).

2.2. Reprocessed SHADOZ Data

Ozone data are taken from the SHADOZ archive (<https://tropo.gsfc.nasa.gov/shadoz>); the profiles measured originate from electrochemical concentration cell ozonesondes coupled to standard radiosondes. For analysis of tropical ozone for the years 1998–2019, we use v06 data from 8 of the 14 long-term stations (Table 1) that are located between 5.8°N and 14°S. For more reliable statistics three of the “stations” or “sites” as they are referred to (Figure 1), are based on combining profiles from pairs of launch locations

Table 1
SHADOZ Site Metadata Including Number of Profiles and Index Terms Used in MLR Ozone Calculations

Trends by layer, % per decade	SC+Para	Natal+Ascen	Nairobi	KL+Java	Samoa
Lat, Lon (°):	-0.92, -89.62/5.8, -55.21	-5.42, -35.38/-7.58, -14.24	-1.27, 36.8	2.73, 101.27/-7.5, 112.6	-14.23, -170.56
Profiles:	1227	1436	941	786	795
MLR Terms:	MEI+QBO	MEI+QBO	MEI+QBO	MEI+QBO+IOD	MEI+QBO
5-10 km					
Jan:	-5.0±8.4% p = 0.233	2.6±5.7% p = 0.357	2.0±8.1% p = 0.639	-0.2±6.8% p = 0.947	7.2±12.3% p = 0.245
Feb:	1.4±9.1% p = 0.764	2.2±5.8% p = 0.445	10.1±8.7% p = 0.018	12.9±7.5% p = 0.001	6.3±12.9% p = 0.322
Mar:	8.1±8.1% p = 0.050	2.1±6.0% p = 0.471	14.2±8.7% p = 0.001	15.7±8.2% p = 0.000	6.0±14.5% p = 0.400
Apr:	6.4±8.4% p = 0.121	3.9±7.4% p = 0.283	6.1±8.2% p = 0.140	3.9±7.1% p = 0.267	2.1±14.7% p = 0.770
May:	-0.0±10.0% p = 0.995	7.2±8.1% p = 0.078	-3.8±7.2% p = 0.297	-3.0±6.2% p = 0.327	-1.3±11.8% p = 0.822
Jun:	-1.1±8.8% p = 0.808	7.4±7.1% p = 0.036	-5.0±6.4% p = 0.125	-2.5±6.5% p = 0.441	-0.6±10.6% p = 0.912
Jul:	1.8±7.4% p = 0.609	4.7±6.1% p = 0.114	-1.3±7.0% p = 0.701	0.0±7.4% p = 0.991	0.4±11.1% p = 0.947
Aug:	3.0±6.5% p = 0.345	0.5±5.3% p = 0.850	0.0±7.5% p = 0.997	1.8±8.2% p = 0.665	-2.5±10.8% p = 0.629
Sep:	3.1±5.8% p = 0.271	-2.6±4.7% p = 0.253	-1.5±7.1% p = 0.679	3.9±7.7% p = 0.317	-5.1±9.9% p = 0.297
Oct:	4.2±6.3% p = 0.183	-2.8±4.5% p = 0.196	-1.1±7.1% p = 0.769	3.3±7.0% p = 0.353	-2.4±9.7% p = 0.624
Nov:	2.8±7.3% p = 0.435	-1.0±4.8% p = 0.668	0.4±7.6% p = 0.923	-1.7±7.4% p = 0.660	3.9±10.5% p = 0.460
Dec:	-2.7±7.5% p = 0.470	1.4±5.2% p = 0.560	0.0±7.6% p = 0.991	-6.0±7.3% p = 0.102	7.7±11.9% p = 0.191
Annual:	1.9±3.1% p = 0.079	1.6±2.3% p = 0.143	1.2±3.1% p = 0.119	1.9±3.0% p = 0.138	1.4±4.7% p = 0.226
10-15 km					
Jan:	-7.7±11.1% p = 0.162	6.7±7.2% p = 0.059	0.1±9.5% p = 0.979	-2.8±7.5% p = 0.456	7.3±19.5% p = 0.448
Feb:	-5.6±11.8% p = 0.336	7.7±7.5% p = 0.042	4.5±10.1% p = 0.350	2.8±7.6% p = 0.466	15.0±20.8% p = 0.147
Mar:	4.8±10.8% p = 0.361	4.9±8.0% p = 0.198	8.8±9.1% p = 0.059	12.9±9.2% p = 0.005	16.5±21.2% p = 0.123
Apr:	12.3±12.4% p = 0.055	2.4±9.9% p = 0.595	7.4±8.8% p = 0.093	15.1±8.5% p = 0.000	12.0±22.0% p = 0.275
May:	4.4±13.4% p = 0.511	3.6±9.5% p = 0.423	2.1±8.5% p = 0.615	5.2±6.9% p = 0.133	2.3±16.3% p = 0.780
Jun:	-3.1±10.0% p = 0.540	6.1±7.6% p = 0.100	0.1±8.3% p = 0.989	-4.5±6.6% p = 0.173	-2.3±12.8% p = 0.720
Jul:	-0.3±8.6% p = 0.942	7.1±7.0% p = 0.044	0.9±9.7% p = 0.838	-7.6±7.7% p = 0.053	-1.8±13.0% p = 0.779
Aug:	6.0±8.4% p = 0.155	5.5±6.6% p = 0.093	-2.3±9.5% p = 0.603	-3.3±10.0% p = 0.500	1.4±13.8% p = 0.841
Sep:	6.7±7.6% p = 0.081	2.2±5.7% p = 0.411	-7.0±7.5% p = 0.062	-1.5±9.4% p = 0.757	1.7±13.9% p = 0.808
Oct:	3.8±8.0% p = 0.343	0.3±5.3% p = 0.919	-6.8±6.2% p = 0.035	-4.7±7.8% p = 0.231	-2.1±14.5% p = 0.778
Nov:	0.5±8.9% p = 0.904	0.4±5.8% p = 0.894	-3.3±6.3% p = 0.271	-6.6±8.5% p = 0.120	-4.2±14.5% p = 0.562
Dec:	-3.2±9.3% p = 0.487	3.0±6.3% p = 0.318	-1.0±7.3% p = 0.780	-5.9±8.8% p = 0.180	-1.1±15.4% p = 0.878
Annual:	1.5±4.0% p = 0.260	3.9±2.8% p = 0.001	-0.2±3.4% p = 0.707	-0.6±3.3% p = 0.347	2.5±6.5% p = 0.243
15-20 km					
Jan:	-1.5±9.1% p = 0.733	2.2±6.1% p = 0.454	3.1±6.9% p = 0.376	-8.8±7.1% p = 0.015	-3.8±8.6% p = 0.377
Feb:	0.8±9.0% p = 0.848	4.5±6.8% p = 0.177	5.5±7.7% p = 0.152	-4.4±8.3% p = 0.289	0.4±9.3% p = 0.929
Mar:	2.9±8.1% p = 0.456	3.1±6.9% p = 0.341	7.3±7.9% p = 0.066	-0.6±8.1% p = 0.898	-0.4±9.8% p = 0.926
Apr:	1.9±8.0% p = 0.623	3.4±7.5% p = 0.329	6.0±7.5% p = 0.110	1.1±8.3% p = 0.795	-5.9±10.2% p = 0.244
May:	-1.6±8.1% p = 0.688	5.2±7.7% p = 0.159	1.2±6.9% p = 0.736	-0.2±7.5% p = 0.942	-6.4±9.7% p = 0.179
Jun:	-4.1±7.0% p = 0.231	1.4±6.8% p = 0.639	-3.3±5.7% p = 0.242	-4.6±6.0% p = 0.122	-2.1±9.0% p = 0.641
Jul:	-5.2±5.6% p = 0.070	-3.8±5.5% p = 0.146	-4.3±5.0% p = 0.089	-9.0±5.5% p = 0.001	-0.4±8.4% p = 0.924
Aug:	-6.1±5.1% p = 0.020	-5.2±4.9% p = 0.040	-2.9±4.9% p = 0.249	-9.3±5.5% p = 0.001	-2.3±7.4% p = 0.525
Sep:	-6.5±5.2% p = 0.013	-2.9±4.9% p = 0.215	-0.9±5.1% p = 0.742	-6.0±5.6% p = 0.035	-3.1±6.9% p = 0.369
Oct:	-5.5±5.8% p = 0.060	-1.6±5.0% p = 0.502	0.2±5.6% p = 0.940	-4.8±6.7% p = 0.151	-2.2±7.1% p = 0.537
Nov:	-3.7±6.7% p = 0.265	-2.6±5.1% p = 0.297	0.6±6.4% p = 0.853	-7.8±7.7% p = 0.043	-2.9±7.4% p = 0.427
Dec:	-2.4±7.8% p = 0.517	-1.8±5.4% p = 0.477	1.4±6.5% p = 0.670	-10.0±7.0% p = 0.005	-5.0±7.8% p = 0.198
Annual:	-3.1±2.8% p = 0.021	-0.4±2.4% p = 0.528	0.6±2.5% p = 0.553	-5.8±2.8% p = 0.000	-2.8±3.4% p = 0.115

Note. Monthly MLR partial column ozone linear trends are shown in percent per decade and include the 95% confidence interval and *p*-value for each trend. Trends with *p*-values < 0.05 are shown in bold and underlined.

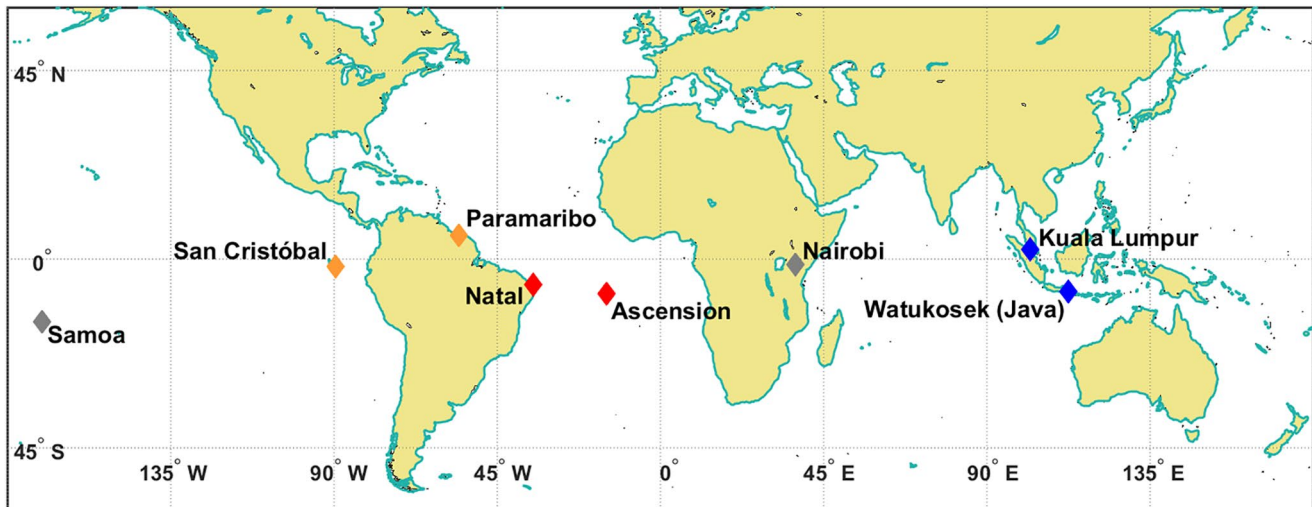


Figure 1. Map of Southern Hemisphere Additional Ozonesondes (SHADOZ) stations used in this study. Stations whose combined records are examined are colored orange (San Cristóbal and Paramaribo), red (Natal and Ascension), and blue (Kuala Lumpur and Watukosek). Samoa and Nairobi records are studied individually and colored gray. Sample numbers appear in Table 1.

abbreviated as follows: SC-Para for San Cristóbal-Paramaribo; Nat-Asc for Natal-Ascension; KL-Java for Kuala Lumpur-Watukosek.

For each station pair in Figures S1–S3 in Supporting Information S1 (left panels), the time series of the ozone column amounts (in Dobson Units, $1 \text{ DU} = 2.69 \times 10^{16} \text{ cm}^{-2}$) at three altitude ranges appear. The ozone column amounts in the lower FT (5–10 km), range from 5 to 15 DU for SC-Para (Figure S1a in Supporting Information S1) but extend from 5 to 20 DU for Nat-Asc (Figure S2a in Supporting Information S1). In the eastern Indian Ocean, over KL-Java (Figure S3a in Supporting Information S1), the ozone columns in the lower FT range from 5 to 10 DU. In the upper FT (10–15 km), the typical lower limit for column ozone is 3 DU at all three sites (Figures S1b, S2b and S3b in Supporting Information S1) but the means show distinct differences: 6 DU at SC-Para; 8.5 DU for Nat-Asc; and <5 DU at KL-Java. The right-side panels for each pair in Figures S1–S3 in Supporting Information S1, that display the mean monthly ozone column amount ($\pm 1\sigma$), further clarify the pairing choices. Jensen et al. (2012) established close similarities of Natal and Ascension FT ozone from 12 years of SHADOZ soundings along with related meteorological factors using self-organizing maps (Section 2.5). Note in Figure S2e in Supporting Information S1 the close agreement of upper FT column ozone at the two stations, especially from August to December when there is a broad seasonal maximum. Although column ozone amounts at Paramaribo (Figure S1e in Supporting Information S1) resemble those of Natal and Ascension in the upper FT (Figure S2e in Supporting Information S1), Paramaribo has a 30%–40% smaller ozone column than Natal and Ascension in the lower FT (cf. Figures S1d and S2d in Supporting Information S1). In the LMS, there is a steady dropoff in SC-Para ozone from September to December (Figure S1f in Supporting Information S1) 16 to 12 DU, that does not occur over Natal and Ascension (cf. Figure S2f in Supporting Information S1). Thus, although Natal is approximately the same distance from Paramaribo and Ascension, the similarities in seasonal ozone patterns argue for pairing Natal with Ascension instead of Paramaribo.

A second approach to pair selection is based on comparing satellite estimates for tropospheric ozone to total tropospheric ozone measured by the sondes. In the upper panel of the frames in Figure S4 in Supporting Information S1, the OMI/MLS estimate of monthly averaged tropospheric column ozone TrCO_{sat} (Ziemke et al., 2006, 2019; $1^\circ \times 1.25^\circ$ product, collocated at the eight tropical SHADOZ sites) is presented with the monthly mean integrated tropospheric column ozone from the sondes, $\text{TrCO}_{\text{sonde}}$. The lower panels in Figure S4 in Supporting Information S1 display the mean offsets of the two TrCO quantities in DU and %, along with the average offset. A scatterplot of all TrCO comparisons for the eight stations (Figure S5a in Supporting Information S1) gives a $r^2 = 0.72$; there is markedly less correlation when TrCO_{sat} and $\text{TrCO}_{\text{sonde}}$ for the four subtropical SHADOZ stations are analyzed (Figure S5b in Supporting Information S1). Regional

Table 2
Same as Table 1, With SHADOZ Site Metadata and Index Terms Used in MLR Ozone Calculations

Trends by layer, % per decade	SC+Para	Natal+Ascen	Nairobi	KL+Java	Samoa
Lat, Lon (°):	-0.92, -89.62/5.8, -55.21	-5.42, -35.38/-7.58, -14.24	-1.27, 36.8	2.73, 101.27/-7.5, 112.6	-14.23, -170.56
Profiles:	1227	1436	941	786	795
MLR Terms:	MEI+QBO	MEI+QBO	MEI+QBO	MEI+QBO+IOD	MEI+QBO
TH-10 to TH-5 km					
Jan:	-7.9±8.9% p = 0.076	3.6±6.4% p = 0.239	-1.8±9.9% p = 0.719	-6.4±7.6% p = 0.092	14.3±17.9% p = 0.110
Feb:	-2.3±9.7% p = 0.624	3.4±6.6% p = 0.275	4.5±10.2% p = 0.374	5.1±8.2% p = 0.215	8.5±17.5% p = 0.320
Mar:	6.0±9.0% p = 0.184	1.9±6.6% p = 0.542	10.1±9.7% p = 0.036	14.4±9.0% p = 0.001	4.2±18.2% p = 0.636
Apr:	5.5±9.5% p = 0.242	3.8±8.4% p = 0.329	5.8±9.2% p = 0.212	10.1±8.2% p = 0.015	3.8±19.9% p = 0.696
May:	-0.4±10.4% p = 0.939	9.7±9.0% p = 0.034	-2.8±8.1% p = 0.495	0.8±7.2% p = 0.813	1.9±15.5% p = 0.802
Jun:	-0.8±8.5% p = 0.841	9.9±7.3% p = 0.013	-4.6±7.3% p = 0.208	-4.8±6.8% p = 0.153	-0.7±12.8% p = 0.921
Jul:	0.9±7.0% p = 0.809	5.7±6.1% p = 0.064	-1.5±7.9% p = 0.701	-6.4±7.4% p = 0.082	-1.8±13.1% p = 0.788
Aug:	-0.0±6.4% p = 0.999	1.0±5.5% p = 0.673	-0.5±8.3% p = 0.896	-4.5±8.9% p = 0.318	-2.0±12.9% p = 0.736
Sep:	-0.6±5.6% p = 0.846	-1.9±4.9% p = 0.416	-2.5±7.8% p = 0.532	0.2±8.5% p = 0.970	-3.5±11.8% p = 0.542
Oct:	1.5±6.2% p = 0.626	-2.9±4.7% p = 0.194	-2.0±7.3% p = 0.585	0.9±7.5% p = 0.813	-4.0±11.8% p = 0.485
Nov:	1.8±7.3% p = 0.607	-2.3±5.0% p = 0.324	-0.2±7.2% p = 0.955	-3.3±8.3% p = 0.420	0.6±13.2% p = 0.921
Dec:	-3.8±7.6% p = 0.309	0.4±5.7% p = 0.878	-1.0±8.1% p = 0.807	-8.7±8.4% p = 0.040	9.8±15.8% p = 0.208
Annual:	-0.1±3.2% p = 0.905	2.0±2.5% p = 0.073	-0.0±3.4% p = 0.955	-0.6±3.2% p = 0.306	1.7±5.9% p = 0.270
TH-5 km to TH					
Jan:	-8.9±11.7% p = 0.127	8.0±6.7% p = 0.021	0.7±8.8% p = 0.863	-4.2±8.5% p = 0.317	9.2±19.3% p = 0.345
Feb:	-5.4±12.2% p = 0.373	10.1±7.6% p = 0.010	5.9±9.8% p = 0.214	3.3±8.3% p = 0.418	10.5±20.1% p = 0.297
Mar:	5.2±11.5% p = 0.365	6.4±7.8% p = 0.097	9.2±9.0% p = 0.042	8.6±9.5% p = 0.072	7.9±19.9% p = 0.424
Apr:	9.5±12.6% p = 0.134	4.0±9.3% p = 0.363	6.5±8.5% p = 0.125	16.5±10.1% p = 0.001	3.5±21.1% p = 0.735
May:	1.7±12.5% p = 0.787	5.7±8.9% p = 0.191	2.1±8.3% p = 0.604	11.6±7.3% p = 0.003	-3.2±16.6% p = 0.699
Jun:	-2.3±10.1% p = 0.648	6.6±7.2% p = 0.066	1.8±7.8% p = 0.651	-1.1±5.9% p = 0.697	-6.1±13.1% p = 0.350
Jul:	0.7±8.9% p = 0.878	6.2±6.4% p = 0.061	3.1±8.7% p = 0.448	-12.5±6.6% p = 0.000	-3.8±13.4% p = 0.563
Aug:	3.7±8.5% p = 0.386	5.5±6.1% p = 0.074	-0.5±8.8% p = 0.905	-13.3±8.4% p = 0.003	0.9±14.4% p = 0.902
Sep:	2.6±7.9% p = 0.505	3.8±5.5% p = 0.162	-5.5±7.4% p = 0.128	-4.7±9.0% p = 0.301	0.6±14.2% p = 0.932
Oct:	1.1±8.9% p = 0.801	1.4±5.2% p = 0.572	-5.4±6.2% p = 0.081	-6.2±8.6% p = 0.149	-4.0±14.2% p = 0.578
Nov:	-0.1±10.1% p = 0.977	0.2±5.4% p = 0.950	-2.7±6.3% p = 0.364	-13.2±8.9% p = 0.004	-4.4±14.3% p = 0.542
Dec:	-4.3±10.1% p = 0.396	2.6±5.6% p = 0.333	-0.9±7.1% p = 0.778	-13.4±9.0% p = 0.004	1.4±15.6% p = 0.861
Annual:	0.2±4.2% p = 0.875	4.7±2.7% p = 0.000	0.7±3.2% p = 0.205	-3.2±3.3% p = 0.055	0.2±6.5% p = 0.922
TH to TH+5 km					
Jan:	-0.6±6.2% p = 0.831	3.2±4.7% p = 0.154	6.5±6.7% p = 0.056	1.5±7.1% p = 0.661	0.8±5.4% p = 0.765
Feb:	0.8±5.9% p = 0.783	4.9±5.0% p = 0.051	2.9±6.7% p = 0.368	1.4±7.1% p = 0.684	1.6±6.2% p = 0.620
Mar:	2.0±5.3% p = 0.434	4.2±4.9% p = 0.087	-1.4±6.6% p = 0.672	-0.3±7.3% p = 0.940	1.3±6.7% p = 0.704
Apr:	2.6±5.5% p = 0.328	2.7±4.9% p = 0.270	-0.4±6.4% p = 0.885	-0.3±7.3% p = 0.934	0.5±6.8% p = 0.896
May:	2.3±6.3% p = 0.455	2.4±5.1% p = 0.332	1.9±6.7% p = 0.550	0.1±7.1% p = 0.965	-2.0±6.5% p = 0.544
Jun:	1.6±6.3% p = 0.608	1.5±5.1% p = 0.535	-0.1±6.8% p = 0.980	-1.4±6.6% p = 0.657	-5.3±6.1% p = 0.083
Jul:	1.2±5.8% p = 0.658	-0.3±4.7% p = 0.892	-2.5±6.5% p = 0.421	-3.1±6.8% p = 0.352	-5.2±5.9% p = 0.073
Aug:	1.0±5.5% p = 0.728	-0.8±4.5% p = 0.713	0.1±6.5% p = 0.974	-2.0±7.5% p = 0.567	-1.5±5.9% p = 0.622
Sep:	0.2±5.3% p = 0.933	0.7±4.4% p = 0.761	4.5±6.7% p = 0.172	0.2±7.8% p = 0.947	1.4±5.9% p = 0.638
Oct:	-0.8±5.3% p = 0.747	1.8±4.2% p = 0.380	4.4±6.5% p = 0.175	-0.1±8.0% p = 0.981	0.3±5.4% p = 0.911
Nov:	-1.6±5.2% p = 0.545	1.5±4.4% p = 0.487	2.7±6.5% p = 0.378	-1.5±8.2% p = 0.703	-1.4±5.0% p = 0.574
Dec:	-1.5±5.4% p = 0.580	1.5±4.5% p = 0.501	4.7±6.7% p = 0.160	-0.6±7.4% p = 0.868	-0.9±4.9% p = 0.711
Annual:	0.6±2.3% p = 0.428	1.9±1.9% p = 0.052	1.9±2.7% p = 0.079	-0.5±3.0% p = 0.621	-0.9±2.4% p = 0.310

Note. Here, the MLR partial column ozone linear trends, in %/decade, are based on FT columns referenced to the tropopause height (TH) -5 km to TH -10 km, for the lower FT, and for the upper FT, the ozone column between the TH and 5 km below the TH. The LMS column ozone is defined by integrating ozone in the region between the TH and 5 km above it. Table S2 in Supporting Information S1 gives the same trends information in DU/decade.

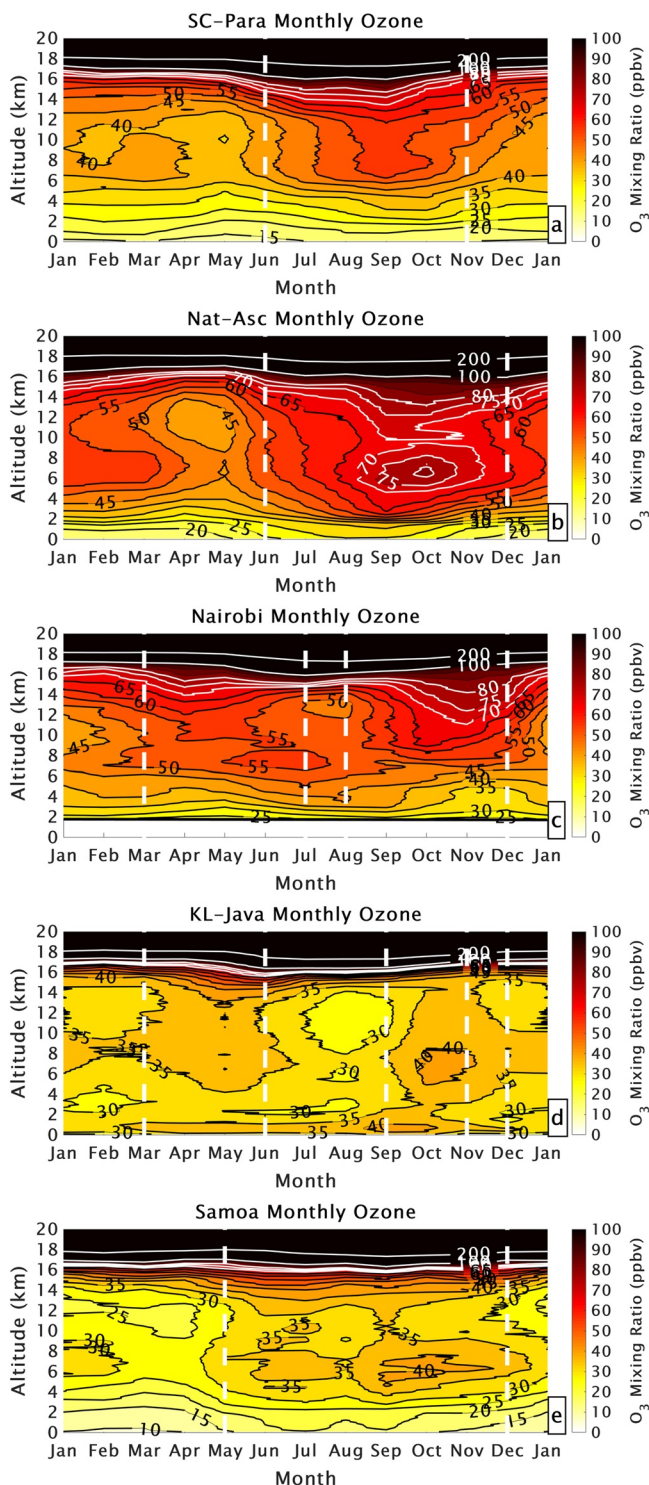


Figure 2. Monthly averaged ozone mixing ratios from the surface to 20-km altitude for the five sites: two individual and three combinations. For clarity, both white and black contours are used for the ozone mixing ratios. White dashed lines indicate transition periods marked by changes in sign of ozone anomalies from annual mean (see Figure 4).

differences in the offset (sonde-satellite in %) support the pairings in Figures S1–S3 in Supporting Information S1. For example, TrCO_{sat} ranges from 6% to 12% low in the eastern Indian Ocean and Atlantic regions but is 3% higher than $\text{TrCO}_{\text{sonde}}$ at Samoa; for Fiji (not shown), TrCO_{sat} exceeds $\text{TrCO}_{\text{sonde}}$ by 6%.

The v06 SHADOZ data, reprocessed in 2016–2018, reduced inhomogeneities due to instrument or data-handling changes (Witte et al., 2017, 2018) such that sonde total ozone column (TOC) amounts agree with ground-based or satellite data within 2% for all but one station. Data from a number of SHADOZ stations display a 3–6% dropoff in TOC after 2013 (Stauffer et al., 2020; Sterling et al., 2018) relative to satellite and/or ground-based readings. For the Costa Rican station (10°N, 84°W), a ~5% dropoff occurs in FT ozone (Stauffer et al., 2020) so those measurements are not used. For the stations analyzed here, the dropoff is confined to readings above 50 hPa (~20 km) and does not affect the results.

2.3. Multiple Linear Regression Model (MLR)

In order to quantify factors leading to seasonal and interannual variability as well as trends, a standard MLR model (original version Stolarski et al., 1991, updated in Ziemke et al., 2019) is applied to monthly mean ozone profiles for the five stations: the three combined sites, Nairobi and Samoa. The reasoning behind the choice of station combinations was summarized in Section 2.2 and Figures S1–S3 in Supporting Information S1. In order to account for any biases that could arise from intersite ozone differences between the chosen pairs, we calculate ozone anomalies from the individual station’s monthly climatology for all profiles before combining the pairs into monthly means and computing the MLR ozone trends. This procedure avoids “false” trends resulting from periods where the data record shifts to being available at only one of two stations (e.g., 2014–2019 at KL-Java; Figure S3 in Supporting Information S1). This same technique is applied to the 380 K potential temperature surface (tropopause height) as discussed below. For consistency, the ozone and tropopause height anomaly calculations are also applied to individual stations, where comparisons of MLR ozone and tropopause height trends without calculating anomalies show negligible differences.

The MLR model includes terms for annual and semiannual cycles and oscillations prevalent in the tropics: QBO, MEI (Multivariate ENSO Index, v2), and IOD DMI (Indian Ocean Dipole Moment Index; only for KL-Java):

$$O_3(t) = A(t) + B(t) + C(t)\text{MEI}(t) + D(t)\text{QBO1}(t) + E(t)\text{QBO2}(t) + F(t)\text{IOD}(t) + \varepsilon(t)$$

where t is month. The coefficients are as follows: A through F include a constant and periodic components with 12, 6, 4, and 3 month cycles, where A represents the mean monthly seasonal cycle and B represents the month-dependent linear trend. The model includes data from the MEIv2 (<https://www.esrl.noaa.gov/psd/enso/mei/>), the two leading QBO EOFs from Singapore monthly mean zonal radiosonde winds at 10, 15, 20, 30, 40, 50, and 70 hPa levels, and IOD DMI (https://psl.noaa.gov/gcos_wgsp/Timeseries/Data/dmi.had.long.data). The $\varepsilon(t)$ is the residual, that is, the difference between the best-fit model and the raw data. Monthly ozone

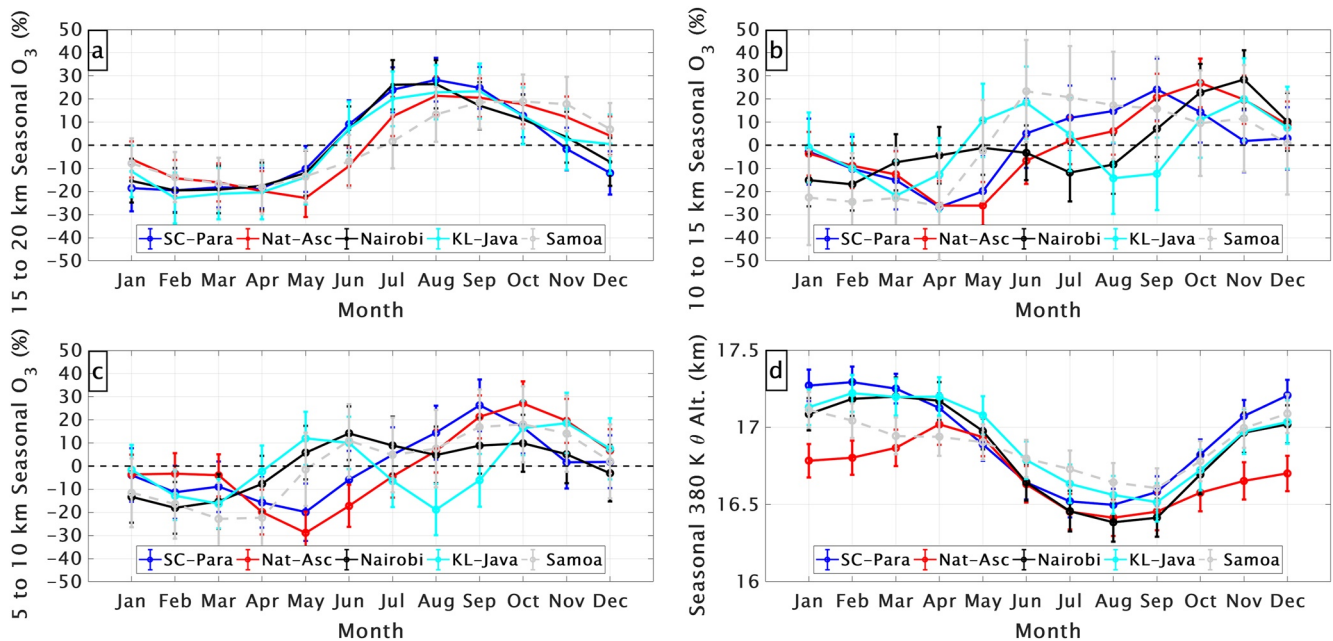


Figure 3. Seasonal ozone variability, expressed as percent anomaly from annual mean, from the Multiple Linear Regression (MLR) model in the lowermost stratospheric (LMS; a), free troposphere (FT; b and c). Tropopause height (TH) anomaly (d, in km) is based on the 380 K potential temperature surface from the radiosondes.

data and model fits for the mid-FT (5–10 km) and LMS (Figures S6 and S7 in Supporting Information S1) are well-correlated; for the LMS, for example, the correlation coefficients are $r = 0.83\text{--}0.90$ (Figure S7 in Supporting Information S1). The IOD DMI term is included for KL-Java because that was the only station where the IOD DMI accounted for an ozone response different from zero with a p -value < 0.05 . The 95% confidence intervals and p -values for each term in the MLR model as presented in this study are determined using a moving-block bootstrap technique (10,000 resamples) in order to account for autocorrelation in the ozone time series (Wilks, 1997). Recent ozone trends studies (Chang et al., 2020; Cooper et al., 2020) have discouraged the practice of distinguishing levels of statistical significance. Therefore, while we focus on ozone trends that are larger than the 95% confidence interval (p -value < 0.05), all trend values, 95% confidence intervals, and p -values are presented in Section 3 (Section 3.2.1, Table 1).

The MLR model was separately applied to the monthly mean ozone profile anomalies at 100-m resolution, and the monthly mean partial column ozone anomaly amounts from 5–10 km, 10–15 km, and 15–20 km. We also applied the MLR model to the monthly mean tropopause altitude anomaly at each station, defined as the 380 K potential temperature surface (e.g., Wargan et al., 2018). It turns out that tropopause height (TH) and LMS ozone trends are strongly correlated. Thus, the MLR analysis was also performed for the ozone column amount anomalies referenced to the tropopause. In that case LMS ozone trends refer to changes in the 5 km above the tropopause with the FT extending from the tropopause to 10 km below the tropopause (Section 3.3.2, Table 2).

2.4. Laminar Identification (LID) and GW Indices

The Laminar Identification (LID) method was used to identify convective signatures in ozone profiles for the 1998–2009 SHADOZ data (Thompson et al., 2011). The LID technique, applied here to the 1998–2019 record (Table 1), is based on the coherence of laminae in each ozone and potential temperature profile pair; laminae are identified as deviations from running means calculated every 0.5 km from surface to 20 km. When the potential temperature and ozone laminae at a given level are strongly correlated ($r > 0.7$), as often occurs in the LMS, the presence of a convectively generated gravity wave (GW) is inferred. The GW occurrence is a proxy for a convective event. Convective influence is quantified by the monthly GW frequency

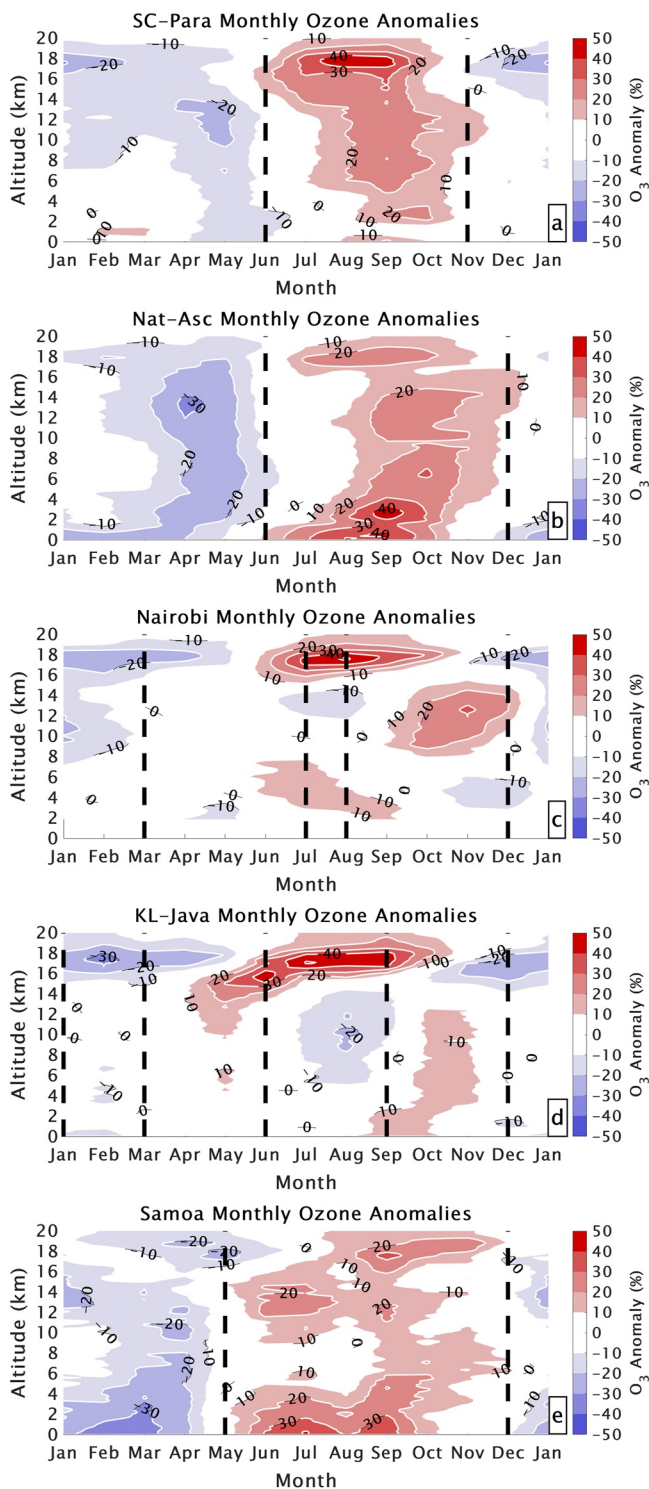


Figure 4. Monthly averaged O_3 mixing ratio anomalies in percent from the annual mean from the surface to 20-km altitude for the two individual and three combination sites. Black dashed lines (same as the white dashed lines in Figure 2) indicate transition periods marked by sign changes to the climatological free troposphere (FT) and lowermost stratospheric (LMS) O_3 amounts (see Section 3.1).

(GWF), defined as the percent ratio of profiles exhibiting the GW signal relative to the total number of profiles within a given month.

2.5. Self-Organizing Maps (SOM)

We have used SOM, a machine-learning technique, to classify ozone profiles in terms of meteorological or chemical influences (Stauffer et al., 2016). The entire set of ozone profiles for each station is ingested into the SOM code to obtain initial nodes (i.e., centroids or means for each cluster) via a linear interpolation between the two largest components of the ensemble. Subsequent iterations assign a given profile to its “best match” until a cluster mean is obtained. We adopt key elements of the procedure in Stauffer et al. (2018): (a) A four-cluster 2×2 SOM is used to avoid clusters with too few members for meaningful statistics (cf. Jensen et al., 2012). (b) SOM clusters are numbered 1–4 based on the cluster “mean” ozone profile. The result is a consistent definition of Cluster 1 and Cluster 4 as “low” and “high” ozone for each site, respectively. Links among SOM ozone profile shape, GWF, and trends are investigated.

3. Results and Discussion

3.1. Seasonal Cycles in Ozone and Convective Influence

Figure 2 displays the 5-site monthly ozone climatology from the surface to 20 km. Regional differences in vertical structure within the FT are pronounced. For example, the contours representing the 60–90 ppbv range never appear in middle FT ozone over KL-Java or Samoa (Figures 2d and 2e). Conversely, FT ozone values ≤ 30 ppbv (light yellows) in the middle FT never appear over the equatorial Americas (SC-Para, Figure 2a), Nat-Asc, or Nairobi (Figures 2b and 2c). These contrasts partly reflect regional differences in ascending versus descending nodes of the Walker circulation. The mean TOC over the south tropical Atlantic Ocean is 5% greater than over the western Pacific, giving rise to the well-known tropospheric zonal wave-one (Thompson, Witte, Oltmans, et al., 2003). Compared to the FT, there is less regional variability in LMS ozone (Figure 8 in Thompson et al., 2017). At all the stations, above ~ 16 km, the colors and contours are similar: nearly uniform over the year with mixing ratio contours of 100 and 200 ppbv similarly spaced.

A large seasonal signal in LMS ozone is associated with the Brewer-Dobson circulation (Figure 3a; cf. Randel et al., 2007). FT ozone seasonality (Figures 3b and 3c) is less uniform due to the timing of various dynamical and chemical influences across sites. However, the minima for all sites occur in January through April or May except for a second short minimum after July over KL-Java. Localized FT ozone maxima occur largely from imported fire pollution: SC-Para in March and after July (Figure 2a); features at 6–8 km over Nat-Asc, Samoa, and KL-Java September to November (Figures 2b–2d); Nairobi (Figure 2c) in June and after August. Month-to-month anomalies from annual mean FT ozone (Figures 3b and 3c) in the 5–10 and 10–15 km layers appear complex for all stations. The vertical dashed lines appearing on Figures 2, 4 and 5 mark when ozone anomalies from the annual mean over 5–15 km change sign, indicating transitions in seasonal

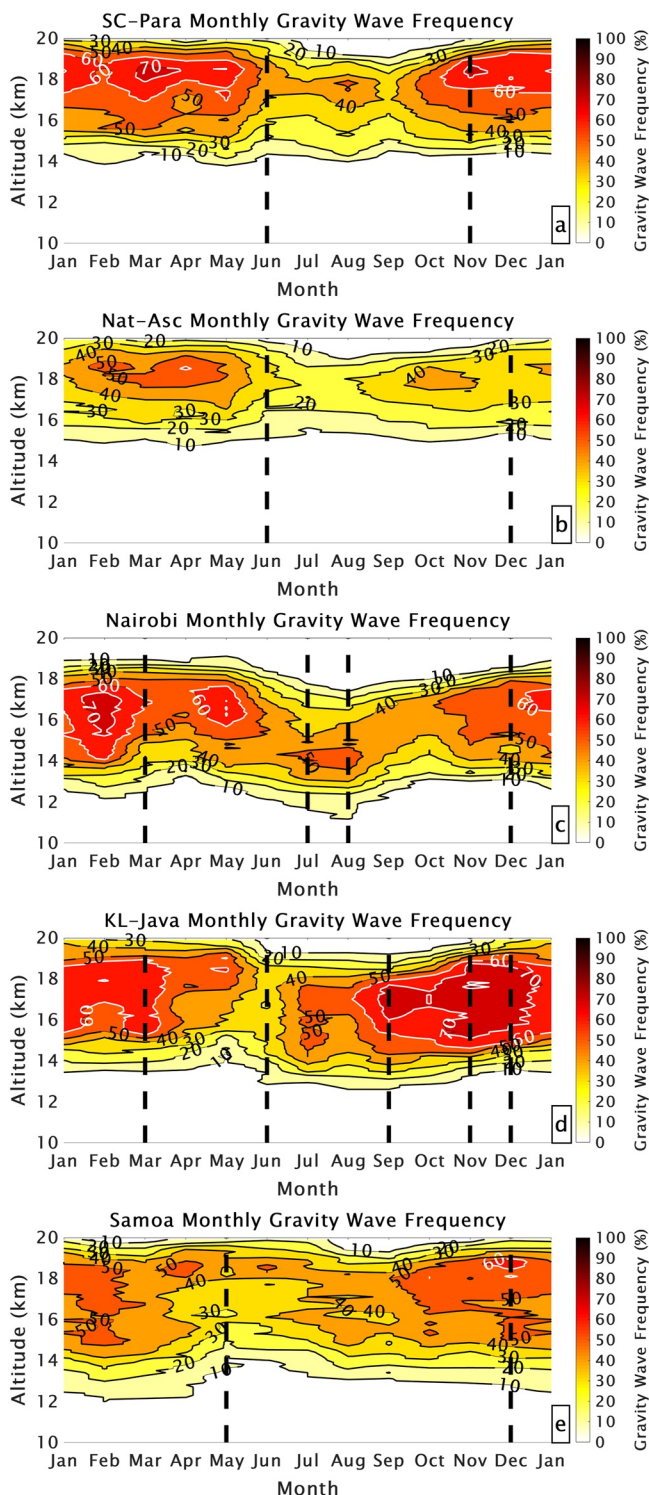


Figure 5. Monthly averaged gravity wave frequency (GWF) in percent from 10 to 20-km altitude corresponding to the profiles in Figure 2 for the two individual and three combination sites. White dashed lines are set by the ozone seasonal transitions as shown as in Figures 2 and 4. The GWF is computed by determining GW effects in percent for each individual profile, and then averaging the results into a monthly frequency.

ozone amount and convective activity. These transitions in ozone anomalies display some regional similarities, for example, the SC-Para and Nat-Asc pairs (Figures 4a and 4b). Nairobi and KL-Java (Figures 4c and 4d), at opposite ends of the Indian Ocean, both exhibit shifts in March and December. Convective influence, given by GWF (Figure 5), with transitions marked as for ozone, shifts during the same periods. GWF reaches 50%–60% during January to April at all locations (Figure 5), during which ozone minima above 8 km, attributed to convective redistribution of near-surface lower ozone air (Figure 2), appear over all stations. Comparing Figures 4 and 5 reveals the correspondence between increased (decreased) convective activity and decreased (increased) ozone amounts, especially in the upper FT and LMS.

3.2. FT Ozone Changes (1998–2019)

In Figure 6, FT and LMS changes in ozone mixing ratio (%/decade during 1998–2019) are displayed, based on monthly mean trends computed with the MLR model. Corresponding values in three layers appear in Table 1. The percentage values in Figure 6 and Table 1 are the result of dividing the MLR $B(t)$ term by the $A(t)$ annual cycle of ozone term. The MLR-calculated $A(t)$ annual cycle derived from monthly mean ozone profiles (i.e., no anomaly calculation) is used to convert the $B(t)$ trend in ppmv/decade (profiles) or DU/decade (partial columns) to %/decade. Ozone trends for both percent/decade and DU/decade are given in Table 1 and Table S1 in Supporting Information S1, respectively (see Section 3.3.2 for Table 2 and Table S2 in Supporting Information S1). Shades of red (blue) in Figure 6 represent ozone increases (decreases); cyan hatching denotes trends with p -values < 0.05. The annual mean trends in Table 1 are computed by taking the average of the 12 monthly trends in DU, and dividing by the mean seasonal ozone in DU to yield the annual percentage trend. Table S1 in Supporting Information S1 presents the trends of Table 1 in DU/decade for the same layers.

3.2.1. FT Ozone Trends: Regional and Seasonal Variability

For all five stations in Figure 6, there is a pattern of strong ozone increase at various altitudes in the FT in February to April or May. In terms of column-integrated ozone amounts for individual stations, these changes range from 0 to +16%/decade (except for SC-Para in February), as displayed in Table 1. However, on an annually averaged basis ozone trends are only +(1–2)%/decade and +(0–4)%/decade in the 5–10 and 10–15 km layers, respectively. Indeed, except for the robust +3.9%/decade over Nat-Asc in the 10–15 km layer, FT ozone increases at the other stations average <2%/decade (Table 1).

Figure 7, that presents monthly mean ozone column changes in the two FT layers, illustrates regional and seasonal variability. For example, the dominant impact of southern African and South American fires on Nat-Asc and Samoa FT ozone in July through November is well-documented (Oltmans et al., 2001; Thompson, Witte, Oltmans, et al., 2003). A near-absence of trends over these sites (Table 1) from July (Samoa) and August (Nat-Asc) through November (Figures 6b and 6e) signifies little change in fires since 1998, consistent with a lack of trends in pyrogenic NO_x over the past 25 years reported in Gaudel et al. (2020; their Figure 5). There is also an increase in 5–10 km ozone over KL-Java (Table 1) in the August to October period, (1.8–3.9)%/decade, which is the typical fire season in

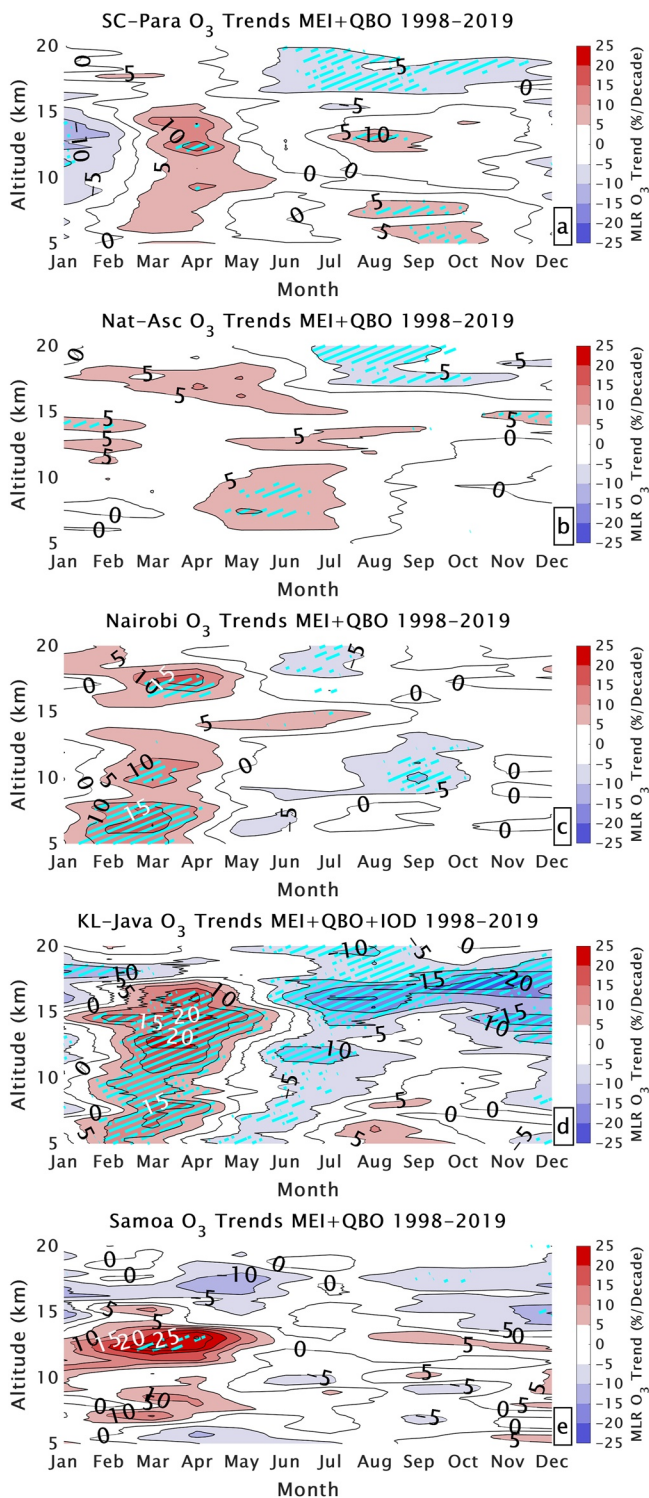


Figure 6. Monthly Multiple Linear Regression (MLR) ozone linear trends from 5 to 20 km in percent per decade for the two individual and three combination sites. Positive trends are shown in red and negative trends are shown in blue. Trends with p -values < 0.05 are shown with cyan hatching.

Indonesia (Pan et al., 2018). The much stronger FT ozone increases over KL-Java (Figure 6d) in February–April, (2.8–15.7)%/decade (Table 1), may be related to the southeast Asian fire season (Liao et al., 2021) and/or to growing urban emissions (Cooper et al., 2020; Gaudel et al., 2020; Zhang et al., 2016).

How do the FT ozone trends based on SHADOZ profiles compare to other analyses? Zhang et al. (2016) and Gaudel et al. (2018) reported on tropospheric ozone changes at different periods within 1994–2015. In both those studies, satellite-derived tropospheric ozone columns and IAGOS commercial aircraft profiles include ozone below 5 km so the results are not directly comparable to the FT SHADOZ-based trends. However, Gaudel et al. (2018; Figures 4 and 24) also presented analysis based on the trajectory-mapped ozonesonde climatology of Liu et al. (2013). Those tropical trends, that included SHADOZ profiles, displayed more regionally varying trends than most satellite products.

In the more recent Gaudel et al. (2020) study, where their IAGOS “Malaysia” data include landing/takeoff profiles at Jakarta, Indonesia, the FT ozone changes over the period 1995–2016 are $\sim +5\%$ /decade. This is about twice the annually averaged increase computed from the SHADOZ KL-Java 5–10 km ozone trends from 1998 to 2019 (Table 1). However, Figure 7 shows that the KL-Java trends are the most seasonally variable of the five stations analyzed. In February through April, the KL-Java trends are $+ (13\text{--}16)\%$ /decade ($p < 0.05$), falling to mostly negative values, $- (2\text{--}8)\%$ /decade, in the 5–10 and 10–15 km layers, the remainder of the year. In Gaudel et al. (2020), the northern tropics is represented by IAGOS profiles over northern South America; the IAGOS Cayenne, French Guiana, landings/takeoffs are not far from Paramaribo. The Cayenne IAGOS trends show a FT ozone increase $\sim 3\%$ /decade. The SHADOZ-based trends at SC-Para on average are $+2\%$ /decade (Table 1). However, as for KL-Java, there is considerable seasonal divergence. In February–April at SC-Para, the FT ozone increase ranges from $+ (1\text{--}12)\%$ /decade, and $+ (3\text{--}7)\%$ /decade August to November (Figure 7). In January, June, and December, the SC-Para trend is actually slightly negative.

A noteworthy point of agreement between the IAGOS and SHADOZ-based records is that in both cases, the largest positive trends (Table 1 and Figure 7) occur at the lowest-ozone season (January to April, Figures 3b and 3c), that is, the minimum ozone amounts have increased over the past several decades. In general, the SHADOZ and IAGOS data provide complementary information on trends. With SHADOZ stations, except for KL-Java, at more remote locations than most IAGOS cities, the SHADOZ results better represent changes in background ozone. The distinctive seasonality of the SHADOZ trends indicates dynamical changes that probably underlie chemical influences that are known to be changing in the tropics (Gaudel et al., 2018, 2020). The next section examines one aspect of possible dynamical influences on the SHADOZ ozone trends.

3.2.2. Role of Convection in FT Ozone Changes

Sections 3.1 and 3.2.1 described an implicit role for convection in the seasonal variability of FT ozone. The annual cycles of FT ozone provide context for the changes shown in Figure 6. The most robust positive FT ozone trends, predominantly from February to May (Table 1 and Figure 7) take place when FT ozone is at its annual minimum (Figures 3b and 3c) and

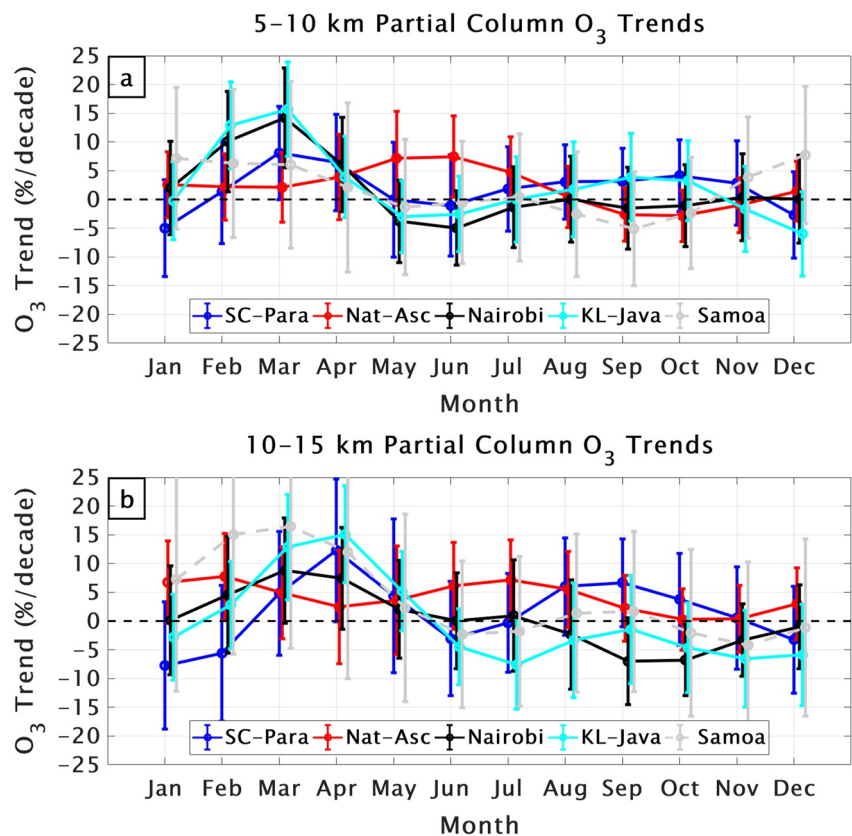


Figure 7. Monthly Multiple Linear Regression (MLR) trends in %/decade for (a) Lower free troposphere (FT) ozone column, integrated from 5 to 10 km, and (b) Upper FT ozone column (10–15 km), derived from Southern Hemisphere Additional Ozonesondes (SHADOZ) sondes. Dots represent the values and the error bars indicate the 95% confidence intervals. Table 1 shows that the annually averaged trend for Nat-Asc at 10–15 km is the only one with $p \leq 0.05$. Note in panel (b) that the Nat-Asc monthly trends are generally lower than for the other four stations in February to May. However, the Nat-Asc ozone increases alone are sustained from June into September.

convective activity is high as signified by GWF (Figure 5). This can be seen when the relationship between ozone profile variability and convection are examined using the LID and SOM methods (Sections 2.4 and 2.5). The classification of ozone profiles for several SHADOZ sites in a 2×2 SOM (Stauffer et al., 2018) established an anticorrelation between FT ozone mixing ratios and convective activity, where the latter was quantified by meteorological parameters at sonde launch time (Figure 7 in Stauffer et al., 2018). The SOM in Figure 8, based on the 5-station data analyzed here, shows similar relationships. Clusters displaying the lowest (Cluster 1) and highest (Cluster 4) profiles of ozone are illustrated. The characteristic S-shapes of FT ozone profiles in Cluster 1 (Figure 8a) display the lowest-mixing ratios whereas much of the elevated ozone in Cluster 4 (Figure 8b) derives from imported pollution at 5–10 km. The GWF corresponding to Cluster 1 (Figure 8c), representing maximum convection, is dominated by January–May profiles (Figure 8e), that is, when there are positive FT ozone changes at all sites. Cluster 4 ozone mixing ratios throughout the FT and LMS (Figure 8b) are much greater than Cluster 1 (Figure 8a) and correspond to the season when the stations are most affected by transported pollution from biomass fires (Figure 8f). The fire season impacts are strongest from June to November except for KL-Java where a March through May maximum corresponds to the southeast Asia burning season (the seasonality can be modified under conditions of a major ENSO; Field et al., 2016; Pan et al., 2018; Thompson et al., 2001). Figure 8d shows that for all stations, convection as indicated by GWF is reduced for the highest-ozone profiles that mostly occur during the burning season: April–May for KL-Java; after July for the other four sites (Figure 8f). GWF in Cluster 4 (Figure 8d) remains above 50% for KL-Java with April and October the most prevalent months (Figure 8f); the latter coincides with the late Asian monsoon period. However, for Cluster 4, the maximum GWF is 47% at Nairobi, com-

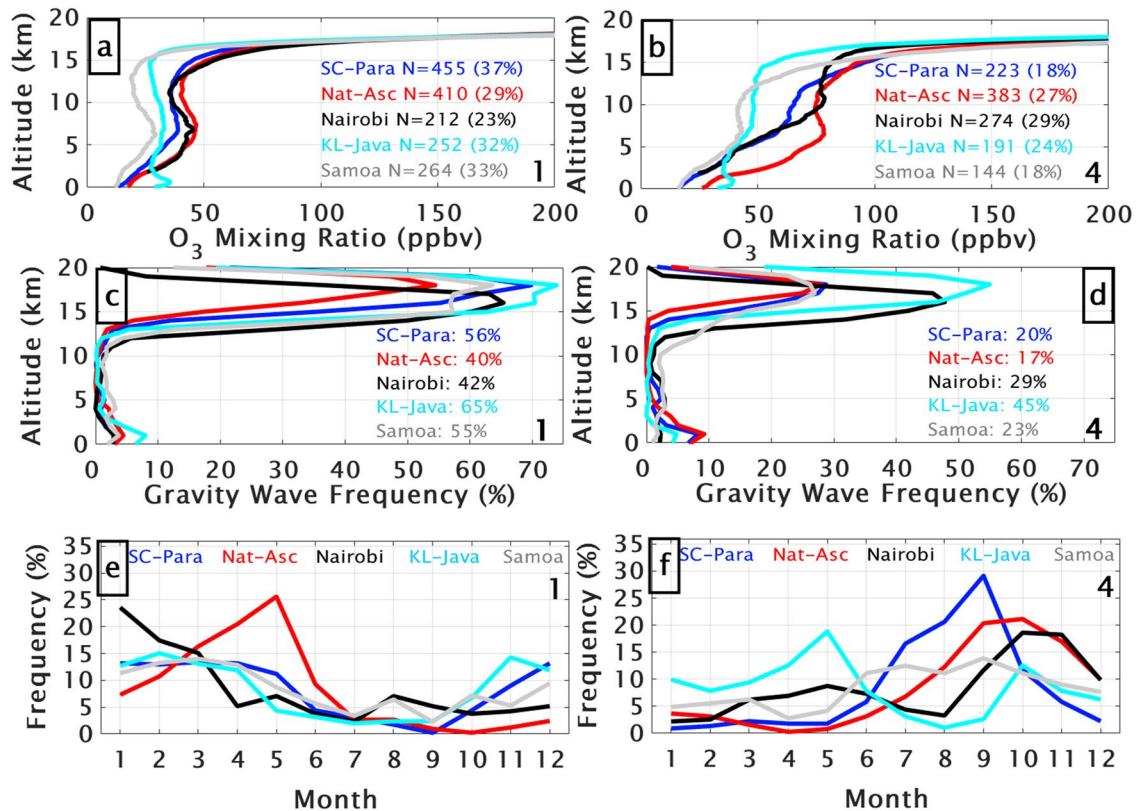


Figure 8. Cluster ozone means for the two individual and three combination sites for Self-Organizing Maps (SOM) Cluster 1 (a) and Cluster 4 (b). The number and percentage of profiles contributing to the clusters appear in each frame and the cluster number is at the lower right. Note that SOM for Clusters 2 and 3 are not shown. (c, d) Gravity wave frequency (GWF in text) as a function of altitude corresponding to SOM Clusters 1 and 4. Average percentage GWF from 15 to 20 km (lowermost stratospheric [LMS]) for each site is shown in the frames. (e) Monthly frequency distribution for the profiles corresponding to SOM Cluster 1. Panel (f) as (e) for Cluster 4.

pared to 64% for Cluster 1 (Figure 8e). For SC-Para, Nat-Asc, and Samoa, the maximum GWF drops below 30% (Figure 8d).

The connection of the ozone trends to convection using the GWF proxy is not clear, but there are correlations among GWF changes and ozone trends. For example, computing the difference in GWF for the first 5 years (1998–2002) and the latest 5 years (2015–2019) in the SHADOZ record (Figure 9) shows correspondence between an increasing GWF trend and decreasing LMS ozone, and decreasing GWF and increasing FT ozone. At all sites, the GWF declines between January and June (Figure 5), albeit weakly at Samoa (Figure 9e), when segments of FT ozone are increasing (Figures 6 and 7). If there is less convection over a station, signifying less vertical mixing and detrainment, FT ozone would accumulate. Midyear, particularly over KL-Java (Figure 9d), GWF increases and there is a corresponding upper FT negative ozone trend (Figure 6d). Whether or not midyear changes in GWF (Figure 9), presumably signifying increases in convection, play a role in LMS ozone and TH trends (Section 3.3.1) is unclear. The interaction among changes in convection and trends in ozone and TH (Section 3.3.2) cannot be determined from the SHADOZ profiles alone. Independent data, for example, OLR, dynamical parameters from reanalyses and model simulations, need to be examined.

3.3. LMS Ozone Trends

3.3.1. LMS Ozone and TH Trends: Seasonal Variability

As for the FT ozone trends, Figure 6 shows distinctive seasonality in LMS ozone trends with layers of 5%/decade losses for 1998–2019 after May at all five stations. At KL-Java (Figure 6d) ozone losses are great-

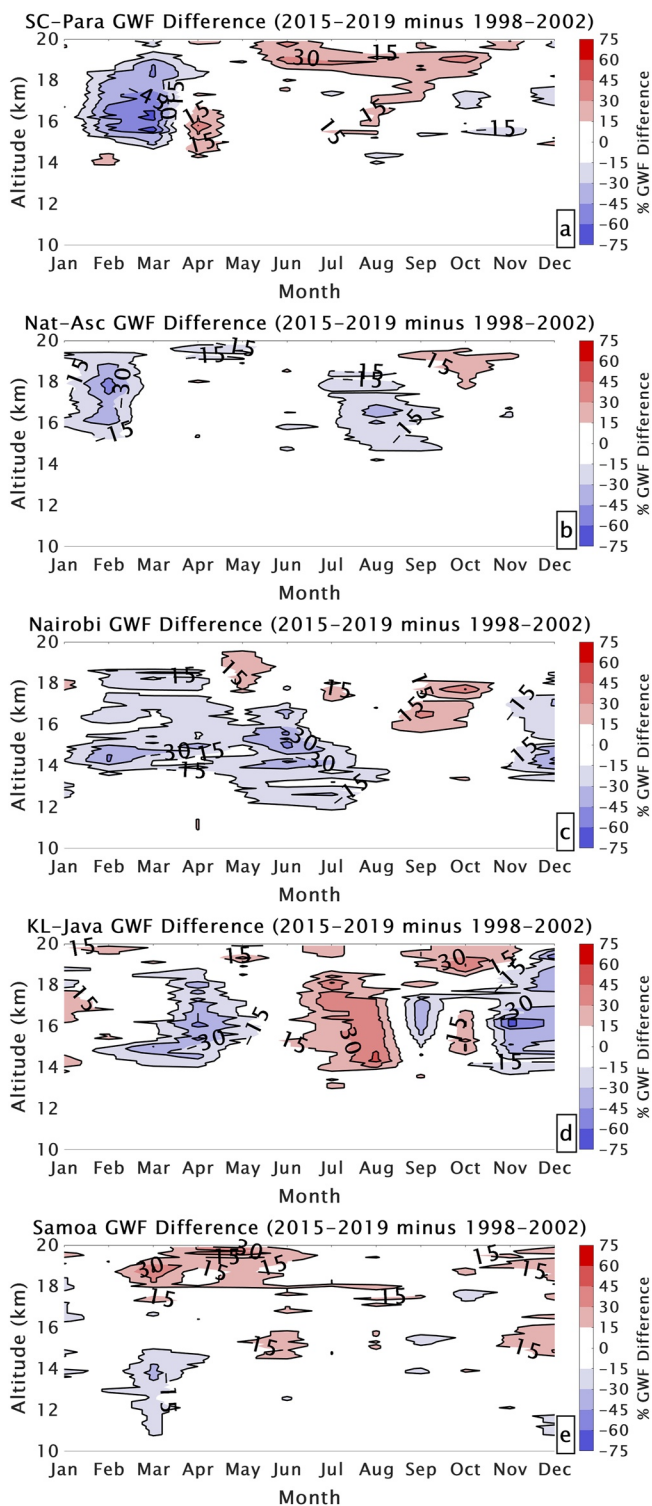


Figure 9. Change in monthly gravity wave frequency (GWF) over two periods (2015–2019 minus 1998–2002) from 10 to 20-km altitude. Increases in GWF are shown in red and decreases in GWF are shown in blue for the two individual and three combination sites.

er, with layers of depletion at 15–20%/decade after August. The corresponding LMS column ozone loss, annually averaged, is $-5.8\%/decade$ (Table 1), almost twice the mean rate over SC-Para (Figure 6a): $-3.1\%/decade$ (Table 1). KL-Java is unique in displaying a layer of ozone loss at 18–19 km in January (Figure 6d). However, there is also a zone of increasing ozone in the LMS over KL-Java March–May between 15 and 18 km. A similar feature, a positive ozone trend at 15–18 km in February–April, appears over Nairobi (Figure 6c). For the Atlantic (Nat-Asc) to Nairobi (Figures 6b and 6c), the most substantial negative trends are found in June through September.

The corresponding ozone column changes from 1998 to 2019 appear in Table 1, where p -values < 0.05 , signified by underlined, bold type, are the most significant. Although isolated months display large LMS ozone losses (to $-10\%/decade$), on an annually averaged basis, only two stations, KL-Java ($[-5.8 \pm 2.8]\%/decade$) and SC-Para ($[-3.1 \pm 2.8]\%/decade$), have significant negative trends. At Samoa ($[-2.8 \pm 3.4]\%/decade$) LMS changes are marginal. There is no LMS ozone loss, on average, over Nat-Asc and Nairobi (Table 1). How do these values compare to the updated satellite-based and model trends reported recently by Ball et al. (2020) who display only zonal averages with no reference to regional variability? Given that the SHADOZ-based LMS trends are positive over large regions and negative over others, the zonally averaged negative trends (Ball et al., 2020) could be overestimating tropical LMS ozone losses.

The first study of seasonality in lower stratospheric ozone trends—results reported as zonal means for four merged satellite products—was published by Szlag et al. (2020). For all four products, the season with the most negative trend is March–April–May, not after June as for the SHADOZ stations in Figure 6 and Table 1. However, the Szlag et al. (2020; Figure 4) calculations may not be directly comparable to our analyses.

In contrast to the highly varied seasonal patterns of FT ozone (Figures 3b and 3c), the annual cycle of LMS ozone (Figure 3a) is fairly uniform (Randel et al., 2007). A comparison with the LMS trends in Figure 6 shows that (a) both positive and negative ozone changes occur during the low-ozone time of year (January to May); (b) more negative, sustained LMS ozone trends take place during the maximum-ozone period (June/July through October/November; Figure 3a). This means that over the year, the magnitude of the LMS seasonal extremes has declined slightly, that is, the annual ozone cycle is flattening.

Figure 10 illustrates the trends in monthly LMS ozone (Figure 10a, $\%/decade$) and TH (Figure 10b, trend in the altitude of 380 K potential temperature [θ] surface in m/decade) as computed from the MLR model for the five SHADOZ stations. After June, when the ozone loss is most pronounced for all stations except Samoa, there is an increase in TH (Figure 10b) that is correlated with the LMS ozone decrease. Figure 3 shows that the annual LMS ozone cycle at Samoa (14°S latitude) differs from the more equatorial stations (5.8°N–7.6°S). The seasonal patterns of the Samoa LMS ozone and TH trends (gray dashed in Figure 10) also diverge from the other stations. There are two periods of LMS ozone loss at Samoa (Figure 10a) with the larger one taking place in April and May. These months of largest ozone loss coincide with the

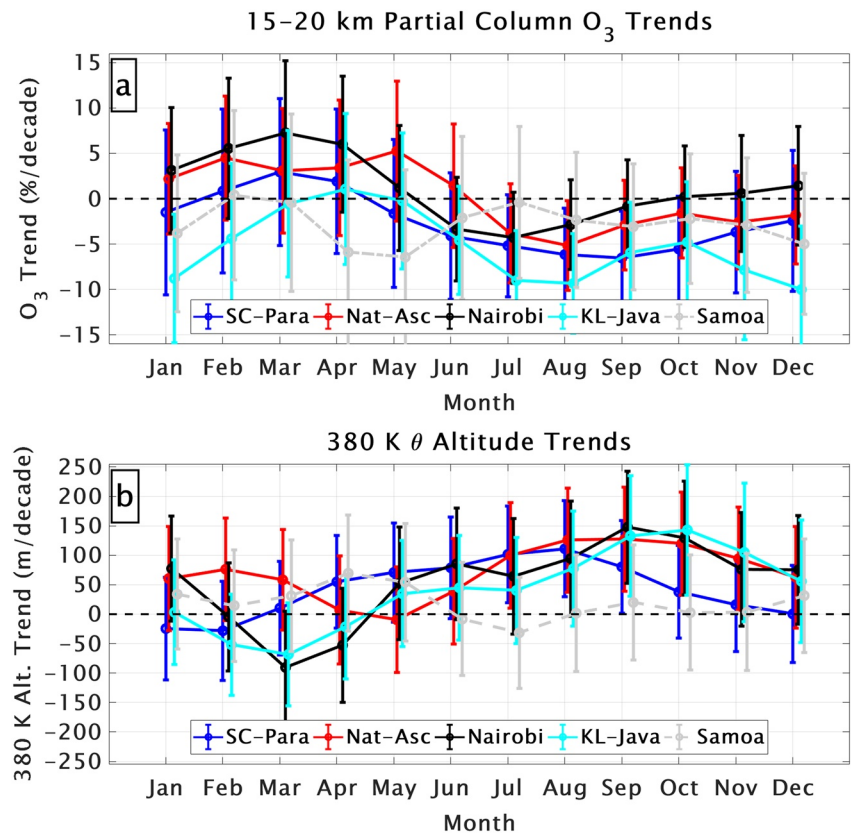


Figure 10. Monthly Multiple Linear Regression (MLR) trends, as %/decade, in (a) Lowermost stratospheric (LMS) ozone column changes (15–20 km) derived from Southern Hemisphere Additional Ozonesondes (SHADOZ) sondes at five stations; (b) Corresponding TH trends from the radiosondes. Dots represent the values and the error bars indicate the 95% confidence intervals.

greatest TH increase at Samoa, although the latter is only 50 m/decade, compared to the 100–150 m/decade increase for the other four stations (Figure 10b).

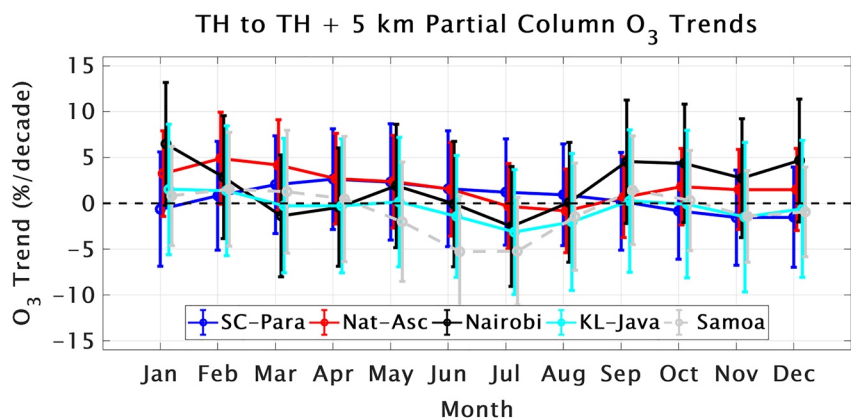


Figure 11. Monthly Multiple Linear Regression (MLR) trends in lowermost stratospheric (LMS) ozone column changes, as %/decade, derived from Southern Hemisphere Additional Ozonesondes (SHADOZ) sondes at five stations, where the LMS column is defined by the amount between the altitude of the tropopause and the tropopause +5 km.

3.3.2. Dynamic Influences in LMS Ozone and Tropopause Height Trends

Because the LMS definition here is 15–20 km, it is reasonable to ask if the increased tropopause height (a stratospheric [tropospheric] thickness reduced [increased] by 50–150 m) is responsible for the negative LMS ozone trend over 1998–2019. To examine this possibility, all ozone profiles were placed in coordinates relative to the 380 K potential temperature surface (TH) prior to calculating monthly means and MLR trends (Section 2.3). Results are presented for layers from 10 to 5 km below the TH, 5 km below the TH to the TH, and the TH to 5 km above the TH (Table 2). Within the 5 km layer above the TH, as displayed in Figure 11, the monthly trends have disappeared for all stations except for small LMS ozone increases at Nat-Asc and Nairobi in the early part of the year, September–December at Nairobi and losses at Samoa in June and July. However, Table 2 does not show significant monthly or mean annual trends in LMS ozone (p -value < 0.05) for any of the SHADOZ stations.

In summary, the annually averaged LMS ozone losses calculated with a fixed-altitude column disappear when the ozone column is determined with a tropopause-defined LMS (Table 2). A perturbed TH, possibly due to a changing climate, is associated with tropical LMS ozone losses from June to November for four stations. The fact that LMS ozone might be increasing over two stations at other times of year underscores the finding that TH influences, and perhaps other dynamical impacts, are not regionally and seasonally uniform. A decisive role for dynamical influences also suggests that where LMS ozone in the tropics is declining (Ball et al., 2018, 2020), the cause is not because of chemical reactions.

4. Summary

The 22-year SHADOZ record (1998–2019) of ozone profiles from five well-distributed tropical regions has been used to compute trends in the FT (5–15 km) and LMS (15–20 km). Both FT and LMS ozone trends exhibit pronounced regional and seasonal variability. We enumerate the major results:

1. There are robust FT ozone increases at all five SHADOZ stations, in thin layers from $\sim(5\text{--}25)\%$ /decade, between February and May. The corresponding FT ozone column amounts typically average $+(3\text{--}10)\%$ /decade during that time; KL-Java is higher. However, both magnitude and direction of these trends vary considerably after May, with individual layers at all stations in the remaining months roughly half positive and half negative. The result is mean trends of $+(1\text{--}4)\%$ /decade, depending on the station.
2. Due to a mismatch in sampling characteristics and time periods investigated, it is difficult to compare SHADOZ trends with those derived from satellite products or aircraft profiles. However, like the IA-GOS-based study of Gaudel et al. (2020) that presented trends from several equatorial locations in South America and southeast Asia, the large SHADOZ FT trends from February to May indicate a shift to higher minimum ozone values. Four of the five SHADOZ stations are very remote and thus represent changes in background ozone. Their nuanced variations in seasonal and regional changes probably signify dynamical changes. As an example, we showed that the FT ozone trends in the early part of the year may be related to reduced convection as indicated by a change in wave activity (GWF).
3. LMS ozone losses mostly take place later in the second half of the year when GWF (convective influence) and tropopause altitude both exhibit increases. The LMS trends are strongest in July to September, reaching $-(4\text{--}9)\%$ /year (ozone) and $+150$ m/decade (TH) at individual stations. Because the LMS ozone loss maximizes at the annual ozone maximum without a comparable increase at other times of year, the ozone cycle associated with the Brewer-Dobson Circulation has been flattening. The TH increase during the annual TH minimum indicates that the annual tropopause cycle is also diminished.
4. When the LMS ozone trends are recomputed using ozone column segments referenced to the changing TH, the ozone losses disappear, even becoming slightly positive at two stations certain months of the year. This finding supports previous analyses that suggest LMS ozone losses since 1998 are dynamically, not chemically, driven.

Randel et al. (2007) and Stolarski et al. (2014) used satellite observations and meteorological analyses to describe multiple dynamical influences on LMS ozone. Our simplified study interprets FT and LMS ozone changes with reference to TH and a proxy for vertical motion that is inferred only from the sounding data. Model diagnostics are required to assess the roles of changing chemistry in the troposphere and to evaluate the contributions of perturbed dynamics to FT and LMS ozone changes. Nonetheless, the relatively small,

geographically distinct changes derived from SHADOZ profiles provide a reference for evaluating (a) LMS ozone trends derived from satellite products that do not include regional variability (Ball et al., 2020; Szelag et al., 2020) and (b) aircraft-based (Gaudel et al., 2020) FT ozone trends. The relatively small SHADOZ trends show that large regions of the tropics do not exhibit year-round FT ozone increases, suggesting that increases in tropospheric ozone in the tropics are partly dynamical in origin and not solely a consequence of growing anthropogenic emissions.

We conclude that using the SHADOZ results to evaluate the regional and seasonal variability of satellite-based products and related models is an impartial way to establish their reliability for ozone trends assessments and predictions of FT and LMS ozone changes in the near future. This first report of an increasing tropopause height over SHADOZ sites is also a reference for satellite observations and models.

Data Availability Statement

SHADOZ v06 profile data are available at <https://tropo.gsfc.nasa.gov/shadoz/Archive.html>. OMI/MLS data are available at https://acd-ext.gsfc.nasa.gov/Data_services/cloud_slice/new_data.html.

Acknowledgments

Support is gratefully acknowledged from the NASA Upper Air Research Program (K. W. Jucks, Program Manager), S-NPP and JPSS (J. F. Gleason, Project Scientist), and the NASA Post-doctoral Program to RMS. The authors are grateful to O. R. Cooper (CIRES/NOAA-CCL) and W. Randel (NCAR) for helpful comments and to suggestions from two reviewers.

References

- Ball, W. T., Alsing, J., Mortlock, D. J., Staehelin, J., Haigh, J. D., Peter, T., et al. (2018). Continuous decline in lower stratospheric ozone offsets ozone layer recovery. *Atmospheric Chemistry and Physics*, 18, 1379–1394. <https://doi.org/10.5194/acp-18-1379-2018>
- Ball, W. T., Chiodo, G., Abalos, M., Alsing, J., & Stenke, A. (2020). Inconsistencies between chemistry-climate models and observed lower stratospheric ozone trends since 1998. *Atmospheric Chemistry and Physics*, 20, 9737–9752. <https://doi.org/10.5194/acp-20-9737-2020>
- Chang, K.-L., Cooper, O. R., Gaudel, A., Petropavlovskikh, I., & Thouret, V. (2020). Statistical regularization for trend detection: An integrated approach for detecting long-term trends from sparse tropospheric ozone profiles. *Atmospheric Chemistry and Physics*, 20, 9915–9938. <https://doi.org/10.5194/acp-20-9915-2020>
- Chipperfield, M. P., Dhomse, S., Hossaini, R., Feng, W., Santee, M. L., Weber, M., et al. (2018). On the cause of recent variations in lower stratospheric ozone. *Geophysical Research Letters*, 45, 5718–5726. <https://doi.org/10.1029/2018GL078071>
- Clain, G., Baray, J. L., Delmas, R., Diab, R., Leclair de Bellevue, J., Keckhut, P., et al. (2009). Tropospheric ozone climatology at two Southern Hemisphere tropical/subtropical sites, (Réunion Island and Irene, South Africa) from ozonesondes, LIDAR, and in situ aircraft measurements. *Atmospheric Chemistry and Physics*, 9, 1723–1734. <https://doi.org/10.5194/acp-9-1723-2009>
- Cooper, O. R., Schultz, M. G., Schröder, S., Chang, K.-L., Gaudel, A., Benite, G. C., et al. (2020). Multi-decadal surface ozone trends at globally distributed remote locations. *Elementa: Science of the Anthropocene*, 8, 23. <https://doi.org/10.1525/elementa.420>
- Field, R. D., van der Werf, G. R., Fanin, T., Fetzer, E. J., Fuller, R., Jethva, H., et al. (2016). Indonesian fire activity and smoke pollution in 2015 show persistent nonlinear sensitivity to El Niño-induced drought. *Proceedings of the National Academy of Sciences of the United States of America*, 113(33), 9204–9209. <https://doi.org/10.1073/pnas.1524888113>
- Folkens, I., Braun, C., Thompson, A. M., & Witte, J. C. (2002). Tropical ozone as an indicator of deep convective outflow. *Journal of Geophysical Research*, 107(D13), 4187. <https://doi.org/10.1029/2001JD001178>
- Folkens, I., Oltmans, S. J., & Thompson, A. M. (2000). Tropical convective outflow and near-surface equivalent potential temperatures. *Geophysical Research Letters*, 27, 2549–2552. <https://doi.org/10.1029/2000GL011524>
- Gaudel, A., Cooper, O. R., Ancellet, G., Barret, B., Boynard, A., Burrows, J. P., et al. (2018). Tropospheric Ozone Assessment Report: Present-day distribution and trends of tropospheric ozone relevant to climate and global atmospheric chemistry model evaluation. *Elementa: Science of the Anthropocene*, 6, 39. <https://doi.org/10.1525/elementa.291>
- Gaudel, A., Cooper, O. R., Chang, K.-L., Bourgeois, I., Ziemke, J. R., Strode, S. A., et al. (2020). Aircraft observations since the 1990s reveal increases of tropospheric ozone at multiple locations across the Northern Hemisphere. *Science Advances*, 6(34), eaba8272. <https://doi.org/10.1126/sciadv.aba8272>
- Grant, W. B., Pierce, R. B., Oltmans, S. J., & Browell, E. V. (1998). Seasonal evolution of total and gravity wave induced laminae in ozone-sonde data in the tropics and subtropics. *Geophysical Research Letters*, 25, 1863–1866. <https://doi.org/10.1029/98GL01297>
- Jensen, A. A., Thompson, A. M., & Schmidlin, F. J. (2012). Classification of Ascension Island and Natal ozonesondes using self-organizing maps. *Journal of Geophysical Research*, 117, D04302. <https://doi.org/10.1029/2011JD016573>
- Lee, S., Shelow, D. M., Thompson, A. M., & Miller, S. K. (2010). QBO and ENSO variability in temperature and ozone from SHADOZ (1998–2005). *Journal of Geophysical Research*, 115, D18105. <https://doi.org/10.1029/2009JD013320>
- Liao, Z., Ling, Z., Gao, M., Sun, J., Zhao, W., Ma, P., et al. (2021). Tropospheric ozone variability over Hong Kong based on recent 20 years (2000–2019) ozonesonde observation. *Journal of Geophysical Research: Atmospheres*, 126, e2020JD033054. <https://doi.org/10.1029/2020JD033054>
- Liu, G., Liu, J., Tarasick, D. W., Fioletov, V. E., Jin, J. J., Moeini, O., et al. (2013). A global tropospheric ozone climatology from trajectory-mapped ozone soundings. *Atmospheric Chemistry and Physics*, 13, 10659–10675. <https://doi.org/10.5194/acp-13-10659-2013>
- Nassar, R., Logan, J. A., Megretskaja, I. A., Murray, L. T., Zhang, L., & Jones, D. B. A. (2009). Analysis of tropical tropospheric ozone, carbon monoxide, and water vapor during the 2006 El Niño using TES observations and the GEOS-Chem model. *Journal of Geophysical Research*, 114, D17304. <https://doi.org/10.1029/2009JD011760>
- Oltmans, S. J., Johnson, B. J., Harris, J. M., Vömel, H., Thompson, A. M., Koshy, K., et al. (2001). Ozone in the Pacific tropical troposphere from ozonesonde observations. *Journal of Geophysical Research*, 106, 32503–32525. <https://doi.org/10.1029/2000JD900834>
- Pan, X., Chin, M., Ichoku, C. M., & Field, R. D. (2018). Connecting Indonesian fires and drought with the type of El Niño and phase of the Indian Ocean Dipole during 1979–2016. *Journal of Geophysical Research: Atmospheres*, 123, 7974–7988. <https://doi.org/10.1029/2018JD028402>

- Randel, W. J., Park, M., Wu, F., & Livesey, N. (2007). A large annual cycle in ozone above the tropical tropopause linked to the Brewer-Dobson circulation. *Journal of the Atmospheric Sciences*, *64*, 4479–4488. <https://doi.org/10.1175/2007JAS2409.1>
- Randel, W. J., & Thompson, A. M. (2011). Interannual variability and trends in tropical ozone derived from SHADOZ ozonesondes and SAGE II satellite data. *Journal of Geophysical Research*, *116*, D07303. <https://doi.org/10.1029/2010JD015195>
- Selkirk, H. B., Vömel, H., Valverde Canossa, J. M., Pfister, L., Diaz, J. A., Fernández, W., et al. (2010). Detailed structure of the tropical upper troposphere and lower stratosphere as revealed by balloon sonde observations of water vapor, ozone, temperature and winds during the NASA TCSP and TC⁴ Campaigns. *Journal of Geophysical Research*, *115*, D00J19. <https://doi.org/10.1029/2009JD013209>
- SPARC/IO3C/GAW. (2019). SPARC/IO3C/GAW report on long-term ozone trends and uncertainties in the stratosphere. In I. Petropavlovskikh, S. Godin-Beekmann, D. Hubert, R. Damadeo, B. Hassler, & V. Sofieva (Eds.), *SPARC report No. 9, GAW report No. 241, WCRP-17/2018*. Retrieved from www.sparc-climate.org/publications/sparc-reports
- Stauffer, R. M., Thompson, A. M., Kollonige, D. E., Witte, J. C., Tarasick, D. W., Davies, J., et al. (2020). A post-2013 dropoff in total ozone at a third of global ozonesonde stations: Electrochemical concentration cell instrument artifacts? *Geophysical Research Letters*, *47*, e2019GL086791. <https://doi.org/10.1029/2019GL086791>
- Stauffer, R. M., Thompson, A. M., Oman, L. D., & Strahan, S. E. (2019). The effects of a changing observing system on MERRA-2-based ozone profile simulations (1980–2016). *Journal of Geophysical Research: Atmospheres*, *124*, 7429–7441. <https://doi.org/10.1002/2018JD030090>
- Stauffer, R. M., Thompson, A. M., & Witte, J. C. (2018). Characterizing global ozonesonde profile variability from surface to the UT/LS with a clustering technique and MERRA-2 reanalysis. *Journal of Geophysical Research: Atmospheres*, *123*, 6213–6229. <https://doi.org/10.1029/2018JD028465>
- Stauffer, R. M., Thompson, A. M., & Young, G. S. (2016). Free tropospheric ozonesonde profiles at long-term U.S. monitoring sites: 1. A climatology based on self-organizing maps. *Journal of Geophysical Research: Atmospheres*, *121*, 1320–1339. <https://doi.org/10.1002/2015JD023641>
- Sterling, C. W., Johnson, B. J., Oltmans, S. J., Smit, H. G. J., Jordan, A. F., Cullis, P. D., et al. (2018). Homogenizing and estimating the uncertainty in NOAA's long-term vertical ozone profile records measured with the electrochemical concentration cell ozonesonde. *Atmospheric Measurement Techniques*, *11*, 3661–3687. <https://doi.org/10.5194/amt-11-3661-2018>
- Stolarski, R. S., Bloomfield, P. R., McPeters, R. D., & Herman, J. R. (1991). Total ozone trends deduced from Nimbus 7 TOMS data. *Geophysical Research Letters*, *18*, 1015–1018. <https://doi.org/10.1029/91GL01302>
- Stolarski, R. S., Waugh, D. W., Wang, L., Oman, L. D., Douglass, A. R., & Newman, P. A. (2014). Seasonal variation of ozone in the tropical lower stratosphere: Southern tropics are different from northern tropics. *Journal of Geophysical Research: Atmospheres*, *119*, 6196–6206. <https://doi.org/10.1002/2013JD021294>
- Swap, R. J., Annegarn, H. J., Suttles, J. T., Haywood, J., Hemlinger, M. C., Hély, C., et al. (2002). The Southern African Regional Science Initiative (SAFARI-2000): Dry-season campaign, an overview. *South African Journal of Science*, *98*, 125–130.
- Szelag, M. E., Sofieva, V. F., Degenstein, D., Roth, C., Davis, S., & Froidevaux, L. (2020). Seasonal stratospheric ozone trends over 2000–2018 derived from several merged data sets. *Atmospheric Chemistry and Physics*, *20*, 7035–7047. <https://doi.org/10.5194/acp-20-7035-2020>
- Thompson, A. M., Allen, A. L., Lee, S., Miller, S. K., & Witte, J. C. (2011). Gravity and Rossby wave signatures in the tropical troposphere and lower stratosphere based on Southern Hemisphere Additional Ozonesondes (SHADOZ), 1998–2007. *Journal of Geophysical Research*, *116*, D05302. <https://doi.org/10.1029/2009JD013429>
- Thompson, A. M., Balashov, N. V., Witte, J. C., Coetzee, J. G. R., Thouret, V., & Posny, F. (2014). Tropospheric ozone increases over the southern Africa region: Bellwether for rapid growth in Southern Hemisphere pollution?. *Atmospheric Chemistry and Physics*, *14*, 9855–9869. <https://doi.org/10.5194/acp-14-9855-2014>
- Thompson, A. M., & Hudson, R. D. (1999). Tropical Tropospheric Ozone (TTO) maps from Nimbus-7 and Earth-Probe TOMS by the modified-residual method: Evaluation with sondes, ENSO signals and trends from Atlantic regional time series. *Journal of Geophysical Research*, *104*, 26961–26975. <https://doi.org/10.1029/1999JD900470>
- Thompson, A. M., Miller, S. K., Tilmes, S., Kollonige, D. W., Witte, J. C., Oltmans, S. J., et al. (2012). Southern Hemisphere Additional Ozonesondes (SHADOZ) tropical ozone climatology: Tropospheric and tropical tropopause layer (TTL) profiles with comparisons to OMI based ozone products. *Journal of Geophysical Research*, *117*, D23301. <https://doi.org/10.1029/2010JD016911>
- Thompson, A. M., Witte, J. C., Hudson, R. D., Guo, H., Herman, J. R., & Fujiwara, M. (2001). Tropical tropospheric ozone and biomass burning. *Science*, *291*, 2128–2132. <https://doi.org/10.1126/science.291.5511.2128>
- Thompson, A. M., Witte, J. C., McPeters, R. D., Oltmans, S. J., Schmidlin, F. J., Logan, J. A., et al. (2003). Southern Hemisphere Additional Ozonesondes (SHADOZ) 1998–2000 tropical ozone climatology. 1. Comparison with TOMS and ground-based measurements. *Journal of Geophysical Research*, *108*(D2), 8238. <https://doi.org/10.1029/2001JD000967>
- Thompson, A. M., Witte, J. C., Oltmans, S. J., Schmidlin, F. J., Logan, J. A., Fujiwara, M., et al. (2003). Southern Hemisphere Additional Ozonesondes (SHADOZ) 1998–2000 tropical ozone climatology. 2. Tropospheric variability and the zonal wave-one. *Journal of Geophysical Research*, *108*(D2), 8241. <https://doi.org/10.1029/2002JD002241>
- Thompson, A. M., Witte, J. C., Sterling, C., Jordan, A., Johnson, B. J., Oltmans, S. J., et al. (2017). First reprocessing of Southern Hemisphere Additional Ozonesondes (SHADOZ) ozone profiles (1998–2016): 2. Comparisons with satellites and ground-based instruments. *Journal of Geophysical Research: Atmospheres*, *122*, 13000–13025. <https://doi.org/10.1002/2017JD027406>
- Thouret, V., Saunio, M., Minga, A., Mariscal, A., Sauvage, B., Soleté, A., et al. (2009). An overview of two years of ozone radio soundings over Cotonou as part of AMMA. *Atmospheric Chemistry and Physics*, *9*, 6157–6174. <https://doi.org/10.5194/acp-9-6157-2009>
- Wargan, K., Orbe, C., Pawson, S., Ziemke, J. R., Oman, L. D., Olsen, M. A., et al. (2018). Recent decline in extratropical lower stratospheric ozone attributed to circulation changes. *Geophysical Research Letters*, *45*, 5166–5176. <https://doi.org/10.1029/2018GL077406>
- Wilks, D. S. (1997). Resampling hypothesis tests for autocorrelated fields. *Journal of Climate*, *10*(1), 65–82. [https://doi.org/10.1175/1520-0442\(1997\)010<0065:RHTEAF>2.0.CO;2](https://doi.org/10.1175/1520-0442(1997)010<0065:RHTEAF>2.0.CO;2)
- Witte, J. C., Schoeberl, M. R., Douglass, A. R., & Thompson, A. M. (2008). The quasi-biennial oscillation in tropical ozone from SHADOZ and HALOE. *Atmospheric Chemistry and Physics*, *8*, 6355–6378. <https://doi.org/10.5194/acp-8-3929-2008>
- Witte, J. C., Thompson, A. M., Smit, H. G. J., Fujiwara, M., Johnson, B. J., & Stübi, R. (2018). First reprocessing of Southern Hemisphere Additional Ozonesondes (SHADOZ) profile records (1998–2016): 3. Methodology and evaluation. *Journal of Geophysical Research: Atmospheres*, *123*, 3243–3268. <https://doi.org/10.1002/2017JD027791>
- Witte, J. C., Thompson, A. M., Smit, H. G. J., Fujiwara, M., Posny, F., Coetzee, G. J. R., et al. (2017). First reprocessing of Southern Hemisphere Additional Ozonesondes (SHADOZ) profile records (1998–2015): 1. Methodology and evaluation. *Journal of Geophysical Research: Atmospheres*, *122*, 6611–6636. <https://doi.org/10.1002/2016JD026403>
- Zhang, Y., Cooper, O. R., Gaudel, A., Thompson, A. M., Nédelec, P., Ogino, S.-Y., & West, J. J. (2016). Equatorward redistribution of emissions dominates the 1980 to 2010 tropospheric ozone change. *Nature Geoscience*, *9*, 875–879. <https://doi.org/10.1038/NNGEO287>

- Ziemke, J. R., & Chandra, S. (2003). A Madden-Julian Oscillation in tropospheric ozone. *Geophysical Research Letters*, *30*(23), 2182. <https://doi.org/10.1029/2003GL018523>
- Ziemke, J. R., Chandra, S., Duncan, B. N., Froidevaux, L., Bhartia, P. K., Levelt, P. F., & Waters, J. W. (2006). Tropospheric ozone determined from Aura OMI and MLS: Evaluation of measurements and comparison with the global modeling initiative's chemical transport model. *Journal of Geophysical Research*, *111*, D19303. <https://doi.org/10.1029/2006JD007089>
- Ziemke, J. R., Oman, L. D., Strode, S. A., Douglass, A. R., Olsen, M. A., McPeters, R. D., et al. (2019). Trends in global tropospheric ozone inferred from a composite record of TOMS/OMI/MLS/OMPS satellite measurements and the MERRA-2 GMI simulation. *Atmospheric Chemistry and Physics*, *19*, 3257–3269. <https://doi.org/10.5194/acp-19-3257-2019>